Renewable Energy 162 (2020) 2344–2360

Contents lists available at ScienceDirect

Renewable Energy

journal homepage: www.elsevier.com/locate/renene

An exploratory study on using Slippery-Liquid-Infused-Porous-Surface (SLIPS) for wind turbine icing mitigation

Liqun Ma, Zichen Zhang, Linyue Gao, Yang Liu, Hui Hu*

Department of Aerospace Engineering, Iowa State University, Ames, IA, 50011, USA

ARTICLE INFO

Article history:
Received 12 May 2020
Received in revised form
18 September 2020
Accepted 3 October 2020
Available online 10 October 2020

Keywords:
Wind turbine icing
SLIPS
Impact ice accretion
Icephobic coatings
Anti-/de-icing

ABSTRACT

An experimental study was conducted to explore the potentials of using a Slippery-Liquid-Infused-Porous-Surface (SLIPS) for wind turbine icing mitigation. The SLIPS was prepared by infusing a lubricant oil into a nanofibrous membrane, which can stick firmly to the surface of a turbine blade model. While the SLIPS was found to effectively suppress impact ice accretion on the blade surface where strong aerodynamic forces are exerted, ice was still found to accrete in the vicinity of the blade stagnation line where aerodynamic forces are at their minimum. A novel hybrid anti-/de-icing strategy to integrate the SLIPS with a minimized leading-edge heating was demonstrated to effectively remove the ice accretion over entire blade surface. An comprehensive experimental study was also performed to evaluate the durability of the SLIPS to resist wearing away of the substrate materials and depletion of the infused lubricant oil due to "rain erosion" effects, in considering its practical usage for wind turbine icing mitigation. It was found that the "rain erosion" effects would induce significant surface wettability degradation, substantial ice adhesion increment and even structural failures to the SLIPS as the duration of the rain erosion testing increases.

1. Introduction

Wind energy is one of the cleanest renewable power sources. The U.S. Department of Energy has challenged the nation to produce 20% of its total power from wind by 2030, and 35% by 2050 [1]. While winters are supposed to be the best season for wind energy harvesting due to the windy seasons and increased air density with the decreasing temperature, wind turbine icing represents the most significant threat to the integrity of wind turbines in cold weather [2–4].

It has been found that, even a light icing event such as frost can produce enough surface roughness on wind turbine blades to reduce their aerodynamic efficiency considerably, resulting in substantial power reduction of the wind turbines [5,6]. In the case of extreme icing, it may not be possible to start the turbine with subsequent loss of all possible production for quite long periods of time – resulting in significant energy loss. One example is a turbine in Sweden that was stopped for over 7 weeks during the best operation period because of icing. The ice-induced energy production losses have been found to reach more than 20% of the annual energy production (AEP) on many wind energy sites with severe icing [7,8].

Wind turbine icing occurs when super-cooled, airborne water droplets, which make up clouds, fog, freezing rain, or drizzle, freeze upon impacting onto turbine surface that allows for the formation of ice. The freezing can be complete or partial, depending on how rapidly the latent heat of fusion can be released into the ambient air. In a dry regime, all the water collected in the impingement area freezes on impact to form *rime ice*, as shown schematically in Fig. 1(a). For a wet regime, only a fraction of the collected water can freeze in the impingement area to form *glaze ice* and the remaining water would run back and freeze in the downstream region outside the impingement area, as revealed in Fig. 1(b). While rime ice is usually associated with colder temperatures (i.e., below −10 °C), lower liquid water contents, and smaller size of the water droplets carried by incoming airflow, glaze ice accretes with warmer temperatures (i.e., above −10 °C), higher liquid water contents, and larger droplet size [9]. Rime ice accretion would closely follow the original contour of the airfoil profiles in general due to the almost instantaneous freezing of the impinging water droplets; therefore, the aerodynamic performance penalties are relatively small, in comparison those induced by glaze ice accretion. Because of its wet

* Corresponding author.
E-mail address: huhui@iastate.edu (H. Hu).

https://doi.org/10.1016/j.renene.2020.10.013
0960-1481/

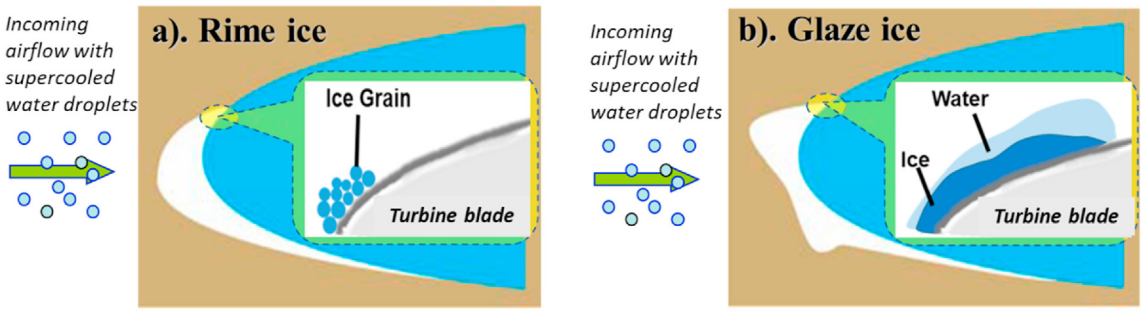

Fig. 1. Rime ice and glaze ice accretion over wind turbine blades.

nature, glaze ice forms much more complicated shapes, and the resulting ice shapes tend to substantially deform the accreting surface with the formation of "horns" and larger "feathers" growing outward into the airflow [10,11]. Glaze ice accretion would severely decrease the aerodynamic performance by causing large-scale flow separation, resulting in dramatic lift reduction and drag increase [12].

Extensive efforts have been undertaken in recent years to develop anti-/de-icing systems for wind turbine icing mitigation [2,5,13,14]. All the anti-/de-icing methods used for wind turbine icing protection can be classified in two categories: active and passive methods. While active methods rely on supplying external energy to the system for the anti-/de-icing operation, passive methods take advantage of surface properties to eliminate or/and prevent ice formation and accretion. Currently, the most-commonly-used wind turbine anti-/de-icing systems are thermal-based approaches, i.e., utilizing electric resistant heating or hot air bleeding to warm up massive surfaces to melt out ice accreted over wind turbine blades [5,15], which are found to be very inefficient and energy consuming. Passive approaches using hydro-/ice-phobic coatings are currently being investigated for use as viable strategies for wind turbine icing mitigation. An ideal solution for wind turbine icing mitigation would be a hybrid system that requires only a minimized power input to effectively delaminate the ice accretion in the required locations, while utilizing passive hydro-/ice-phobic coatings to reject ice accretion in regions with the requisite aerodynamic forces [16].

Inspired by the outstanding self-cleaning capability of lotus leaf and duck feather, extensive studies have been conducted in recent years to develop coatings to make ***S**uper-**h**ydrophobic **S**urfaces* (**SHS**) [17,18], on which water droplets bead up with a very large contact angle (i.e., >150°) and drip off rapidly when the surface is slightly inclined. One attractive application of SHS, in addition to the extraordinary water-repellency, is their potentials to reduce snow/ice accumulation on solid surfaces. Under a frost-free environment (i.e., low humidity conditions), SHS were found to show promising behaviors in delaying ice formation [19] even at temperatures as low as −25 to −30 °C [20].

It is well known that, all superhydrophobic materials/surfaces possess textured or rough surfaces [21,22]. As revealed schematically in Fig. 2, when a macroscopic water droplet comes in contact with a textured super-hydrophobic material/surface, it adopts the so-called ***Cassie-Baxter state*** [23] with air trapped in the surface texture beneath the droplet. Since the macroscopic water droplet is supported on thousands of pockets of air, it beads up and displays very high contact angles (typically > 150° for SHS). However, microscopic water droplets can condense from the surrounding humid air within the surface textures of the super-hydrophobic surfaces to form so-called ***Wenzel state*** [24], with water completely wetting the pores or asperities of the textures. Furthermore, for the wind turbine icing scenario, water droplets would impact onto blade surface at high speed up to ~90 m/s near blade tips for utility-scale wind turbines. The impacted water droplets would readily penetrate the surface textures to promote the transition from Cassie-Baster state to fully wetted Wenzel state. Once water freezes within the textures in the Wenzel state, it is extremely difficult to remove the ice, even more than on non-textured surfaces, because of the interlocking between ice and the textures [25,26]. Consequently, some SHS were found to display even higher ice adhesion strengths, in comparison to non-treated surfaces, substantially increasing the amount of energy required to remove the accumulated ice [22,27]. In summary, SHS coatings with textured surfaces that are effectively ice-phobic at nominal static icing conditions may not perform well for the applications of wind turbine icing scenario involving in impingement of super-cooled water droplets onto blade surfaces at high impacting speeds.

Another strategy to reduce ice adhesion strength to a solid surface is to use a layer of liquid lubricant, which is immiscible with water, between ice and the solid surface. The use of such lubricated surfaces was investigated as early as 1960s [28], and has gained increasing attentions again recently with the introduction of a concept called Slippery Liquid-Infused Porous Surfaces (SLIPS) [29,30]. The SLIPS concept is inspired by the Nepenthes pitcher plants, which have evolved highly slippery, liquid-infused micro-textured rim to capture insects [31]. As shown schematically in Fig. 3, a SLIPS consists of a continuous film of lubricating liquid locked in place by a micro/nano-structured substrate, which can repel immiscible liquids that come into contact. The premise of the SLIPS design is that a lubricated surface is intrinsically smooth and defect-free down to the molecular scale and provides immediate self-repair by wicking into damaged sites via the underlying substrate. The lubricant oil is largely incompressible; and can be chosen to repel immiscible liquids of virtually any surface tension. Owing to its ultra-smooth surface, SLIPS exhibits many features that outperform conventional SHS coatings [30,32], which include very small adhesion to various liquids; rapid and repeatable self-healing; super-repellency at extreme pressure (up to ~676 atm); low adhesion to insects, graffiti, and synthetic adhesives [33,34]. SLIPS-coated surfaces were not only found to be able to suppress ice/frost accretion by effectively removing condensed moisture even in high humidity conditions, but also exhibit at least an order of magnitude lower ice adhesion than the state-of-the-art SHS coatings [35]. Since the inception of SLIPS, it has inspired a number of coating technologies utilizing infused liquids on or within solids surfaces for enhanced anti-icing performance, which include hygroscopic structured surfaces [36,37], magnetic slippery surfaces [38] and soft, so-gel materials/surfaces [39–41].

In spite of the noticeable advances made in the development of various SLIPS with ultra-low ice adhesion strength, most of the engineered slippery surfaces were tested only in a relatively static

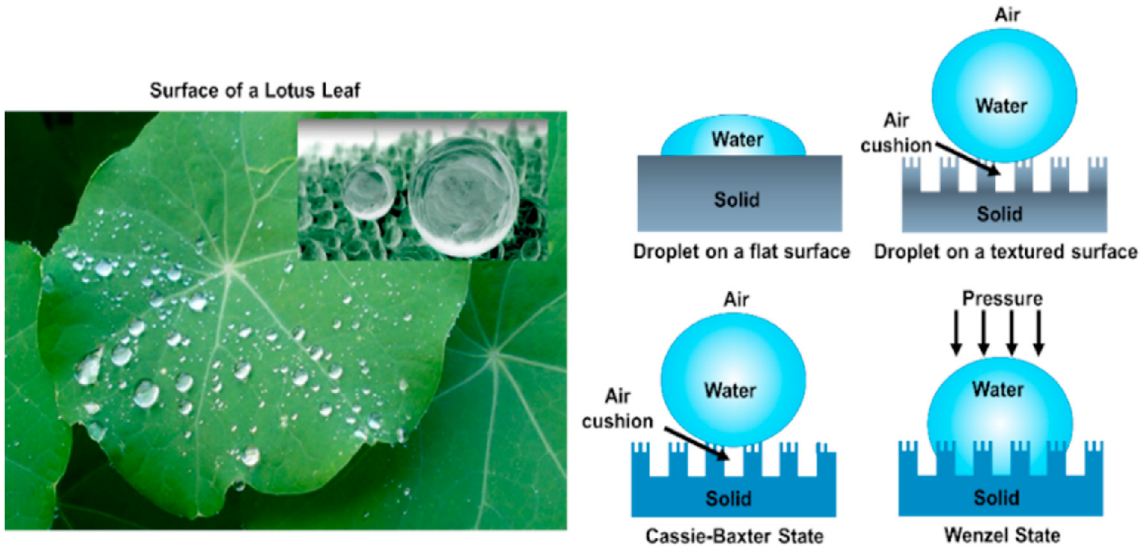

Fig. 2. Super-Hydrophobic Surface (SHS) with nano-/micro-scale surface textures.

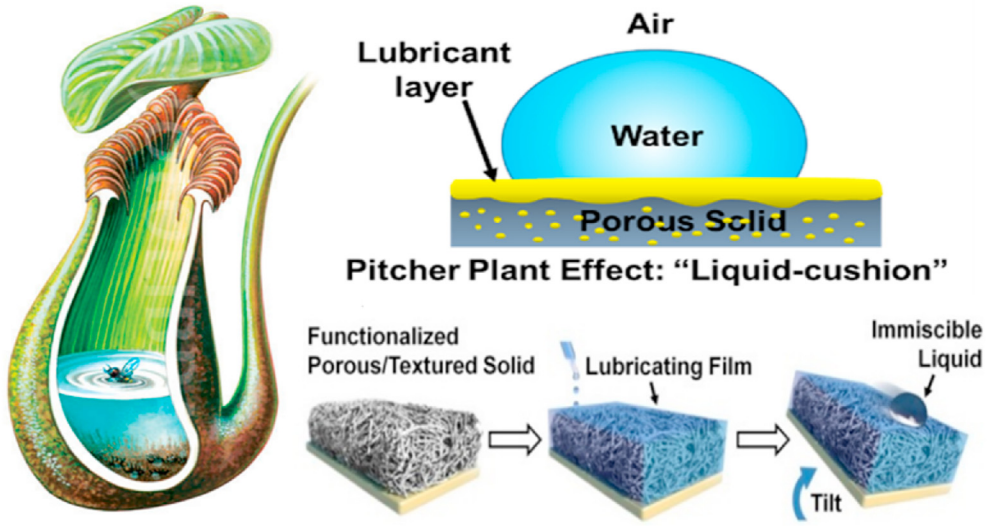

Fig. 3. Schematics of pitcher-plant-inspired slippery-liquid-infused-porous-surface (SLIPS).

environment (i.e., by hand spraying water droplets or pouring water onto SLIPS and then freezing the test samples in refrigerators) [41,42]. SLIPS coated surfaces have not been evaluated under aerodynamic relevant, "*impact icing*" conditions pertinent to wind turbine icing phenomena. Here, the concept of "*impact icing*" is defined as ice formed due to the dynamic collision of water droplets onto a surface at high impact speeds [43,44]. The ice structures accreted under impact icing conditions can vary considerably depending upon the conditions in which the ice is formed. Air temperature, air speed, water droplet size, liquid water content, and geometry of turbine blades could all affect the ice structures that accrete [45].

It should also be noted that, one of the major concerns about using SLIPS for wind turbine anti-/de-icing applications is the sacrificial nature of the liquid lubricant. The infused lubricant liquid may be depleted by evaporation at elevated temperature or at reduced pressure [46]. As ice slides past the lubricated surface, a portion of the liquid lubricant may also be shaved off by the surface of ice (i.e., cohesive failure), demoting the longevity of the lubricated materials [40]. Another concern is the durability of SLIPS upon mechanical contact, which can also potentially damage the substrate and deplete the infused liquid, degrading the integrity of the SLIPS [46]. Furthermore, since wind turbines would be exposed to the high-speed impingement of super-cooled water droplets for a relatively long time in winters, the "rain erosion" resistance performance of SLIPS (i.e., the ability to prevent the wearing of the substrate materials and depletion of infused lubricant liquid by the continuous impingement of water droplets) would be very critical in considering practical applications of SLIPS for wind turbine icing mitigation.

In the present study, an experimental investigation was conducted to explore the potential of SLIPS to mitigate impact icing process over the surface of a typical turbine blade model. The SLIPS was prepared by infusing a lubricant oil of DuPont's Krytox® 103 into a porous layer of nanofibrous Polytetrafluoroethylene (PTFE) membrane, which can stick firmly to the surface of the turbine blade model. The impinging dynamics of water droplets onto the SLIPS coated test surface at a high Weber number of $We \approx 4000$

(i.e., in the range associated with wind turbine icing phenomena) was examined at first, in comparison to that of the test case with an uncoated test surface. By leveraging the Icing Research Tunnel of Iowa State University (i.e., ISU-IRT), the effects of the SLIPS on the impact ice accretion process over the surface of the turbine blade model were investigated, in comparison to that on the uncoated blade surface, to elucidate the fundamental mechanisms how and why the SLIPS can suppress impact ice accretion. In considering potential practical applications of SLIPS for wind turbine icing mitigation, an experimental campaign was also performed to examine the durability of SLIPS to resist "rain erosion" effects. The rain erosion testing aims to evaluate the capability of the SLIPS to prevent the wearing of the substrate material and depletion of infused lubricant oil induced by the continuous impingement of water spray flows at high impacting speeds up to ~90 m/s, simulating the scenario of airborne water droplets impinging onto blade surfaces in the outbound regions near blade tips of utility-scale wind turbines. The time evolutions of the surface wettability (i.e., in terms of the advancing and receding contact angles of water droplets) and ice adhesion strengths on the SLIPS as a function of the rain erosion testing duration were characterized under different testing conditions. The damage patterns of the SLIPS induced by the rain erosion effects were also examined based on analyzing the acquired images of the eroded SLIPS after undergoing rain erosion test experiments. The surface wettability degradation and ice adhesion strength increment are correlated with the damage patterns to elucidate the underlying physics for a better understanding about the characteristics of the rain erosion damages to the SLIPS. To the authors' best knowledge, the work described here is the first to explore/demonstrate the feasibility of using SLIPS to suppress the impact ice accretion process due to the dynamic collision of water droplets onto turbine blade surfaces for wind turbine icing mitigation. It is also believed to be the first comprehensive study to examine the rain erosion characteristics of SLIPS coated surface due to the continuous impingement of water droplets at high impacting speed pertinent to wind turbine icing phenomena.

2. Preparation of SLIPS and measurement systems

2.1. Preparation of SLIPS

Following up the work described in Wong et al. [30], SLIPS used in the present study was prepared by covering the top surfaces of test models with thin porous layers. As shown schematically in Fig. 4, the porous layer used in the present study is a hydrophobic, nanofibrous, Polytetrafluoroethylene (PTFE) membrane purchased from Sterlitech™, which has an average pore size of less than 200 nm. The porous layer has a polypropylene backer which can stick firmly onto the surfaces of the test models. The lubricant fluid used here is Krytox® 103, which is a clear, colorless perfluorinated oil and purchased from DuPont™. As suggested by Wong et al. [30], excess lubricant oil was applied in preparing the SLIPS with the thickness of the excess oil film over the porous layer being 60–80 μm. It should be noted that, the slippery oil of Krytox® 103 was also used by Wong et al. [30] and Liu et al. [47] to make SLIPS due to its low evaporation rate, thereby, minimizing the influence of oil depletion from evaporation. Based on the experimental results reported by Wong et al. [30], the evaporation rate of Krytox® 103 was found to be less than 0.05% per day, and the changing of the surface wetting property was negligible within a 28-day period. Therefore, the changes in the surface wettability and durability of the SLIPS due to the evaporation of the perfluorinated oil is believed to be negligible for the cases of the present study.

2.2. Measurements of the contact angles and ice adhesion strength

In the present study, the contact angles (CA) of water droplets (i.e., static CA θ_{static}; advancing CA $\theta_{adv.}$, and receding CA θ_{rec}) on the test plates with and without the SLIPS were measured by using a similar needle-in-the-sessile-drop method as that described in Korhonen et al. [48]. Fig. 5 gives the experimental setup to quantify the CA values of water droplets on the test plates. While the static CA values were measured by placing sessile water droplets (~50 μL deionized water in volume) on the test plates, the advancing and receding CA values were measured by expanding and contracting the water droplets with a rate of 10 μL/s. The expanding and contracting of the water droplets were controlled by using a programmable Syringe pump (Genie Touch™). A digital camera (PCO2000 with 2000 pixels × 2000 pixels in spatial resolution) with a 12 × zoom lens system (LaVision) was used to record the droplet images to determine the CA values. A MATLAB-based image processing software package was developed "in-house" to determine the CA values from the recorded droplet images. The CA measurements were repeated 10 times for each test case to minimize the measurement errors, which were estimated to be within ±3°.

It should be noted that, the test plates used in the present study are made of polymer-composite materials, i.e., the similar materials as those to make of utility-scaled wind turbines. Table 1 summarizes the measured static, receding and advancing CA results of water droplets on the polymer-composite-based test plate before and after coated with SLIPS. It can be seen clearly that, before applying the SLIPS to coat/cover the test plate, the static CA of water droplets on the test plate was found to be obviously smaller than 90° (i.e., $\theta_{static} \approx 65°$), confirming the hydrophilic nature of the polymer-composite-based test plate. The corresponding CAH value

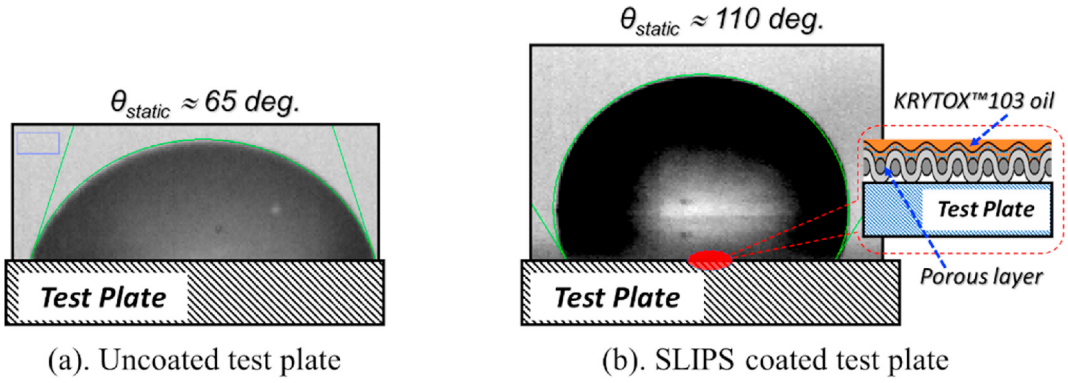

Fig. 4. Water droplets on the test plates before and after coated with SLIPS.

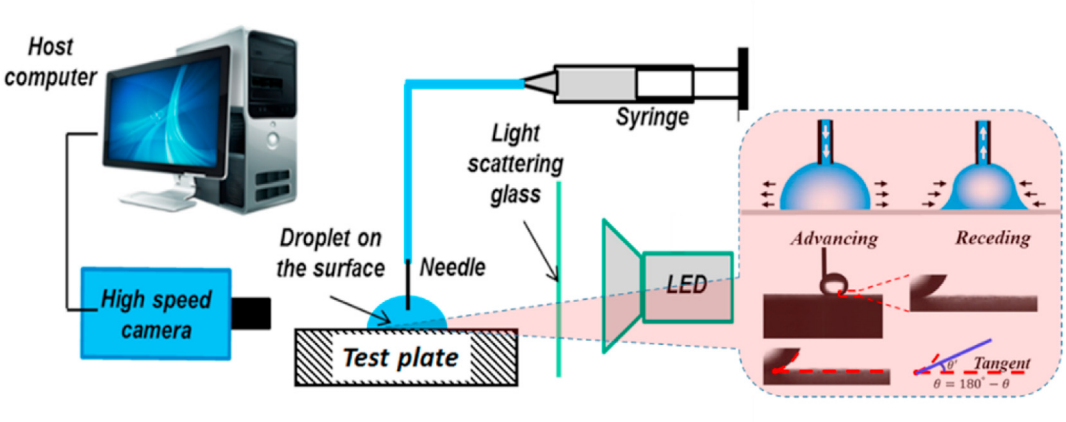

Fig. 5. The experimental setup to measure contact angles of water droplets on the test surfaces.

Table 1
Contact angles & ice adhesion strength on the test plates before erosion testing.

Studied Surface	Wettability	Static CA θ_{static}	Advancing CA, θ_{adv}	Receding CA, θ_{rec}	CAH value	Ice adhesion strength (KPa)
Uncoated Test plate	Hydrophilic	~65°	~105°	~45°	~60°	~1400
SLIPS coated test plate	Hydrophobic	~110°	~115°	~98°	~7°	~35

(i.e., the difference between the advancing and receding contact angles of water droplets, $CAH = \theta_{adv} - \theta_{rec}$) was found to be quite big, i.e. $CAH \approx 60°$, on the uncoated test plate.

After applying the SLIPS to coat/cover the test plate, while the static CA of the water droplet on the SLIPS was found to be $\theta_{static} \approx 110°$, and the corresponding CAH value was found to decrease to $CAH \approx 7°$. The measured CA values were found to agree well with those reported in Wong et al. [30]. It should be noted that, CAH value usually refers to the surface slipperiness to quantify the tendency of a water droplet to bounce and/or roll off the surface. The smaller CAH value is, the easier water droplets will be to bounce and/or roll off from the surface. For the wind turbine icing scenario, wind turbine blades with a smaller CAH value are highly desirable, since a smaller CAH value would imply more readily bouncing and rolling off of the impacting water droplets from the blade surface, thereby, less ice accretion on the blade surface.

By using a similar measurement system as the one used by Mueller et al. [49], the ice adhesion strengths, τ_{ice}, on the SLIPS coated and uncoated test plates were also measured before and after undergoing rain erosion testing. All the ice adhesion measurements were conducted in a temperature controllable testing chamber. While the surface temperatures of the test plates were maintained at $T_w = -5.0$ °C, the ice adhesion measurements were repeated ~10 times for each test cases. The measured ice adhesion strengths on the test plates with and without the SLIPS are also listed in Table 1. It can be seen clearly that, while the ice adhesion strength on the uncoated, polymer-composite-based test plate (i.e., before applying the SLIPS) was found to be ~1400 kPa, the ice adhesion strength on the SLIPS coated surface was found to be only $\tau_{ice} \approx 35$ kPa, which is only about 2.5% of the corresponding value on the bare polymer-composite-based test surface.

3. Experimental results and discussions

3.1. Impinging dynamics of water droplets onto test plates with and without the SLIPS

Since the impingement of supercooled water droplets onto the wind turbine blades is directly related to the total amount of the impact ice accreted on the turbine blades, an experimental investigation was conducted in the present study to examine the effects of the SLIPS on the impinging dynamics of water droplets by providing a side-by-side comparison of the transient behaviors of the impinging droplets on a SLIPS coated test plate to those on an uncoated test plate.

It is well known that Weber number (We), which can be thought of as a measure of the relative importance of the droplet inertia compared to its surface tension, is widely used to characterize impinging dynamics of droplets. Weber number (We) is defines as $We = \rho V_\infty^2 D/\sigma$, where ρ is the density of a droplet (kg/m^3); V_∞ is the velocity of the droplet (m/s); D is the droplet diameter (m); and σ is the surface tension (N/m). For a typical wind turbine icing scenario, with the super-cooled water droplets in the incoming airflow being about 20–100 μm, and nominal droplet impacting speed of being $V_\infty \approx 60$ m/s or greater in the outbound region of wind turbine blades, the corresponding Weber number would be about 3000 or greater (i.e., $We > 3000$). While several studies were conducted to demonstrate the promising performance of SLIPS in delaying ice formation, almost of the previous studies were conducted in a relatively static environment. The corresponding values of the Weber numbers were found to be very small (i.e., We < 100) [50–52], which is at least 1–2 orders of magnitude smaller than the associated Weber numbers of the impacting water droplets pertinent to wind turbine icing phenomena.

In the present study, a specially-designed vertical wind tunnel was used to accelerate the water droplets exhausted from a droplet generator to enable the droplet impingement experiments to be performed at high Weber numbers (i.e., $We \approx 4000$) relevant to wind turbine icing phenomena [3,43]. Fig. 6 shows the schematic of the experimental setup used to study the dynamic droplet impacting process. The vertical wind tunnel is composed of an air settling section, a contraction section, a test section, connecting duct systems, and a ducted fan. The ducted fan (JP70 EDF Lipo), which was powered by a power supply unit (Volteq HY30100EX) and a rotational speed controller, was used to drive the airflow inside the vertical wind tunnel. Water droplets out of the droplet

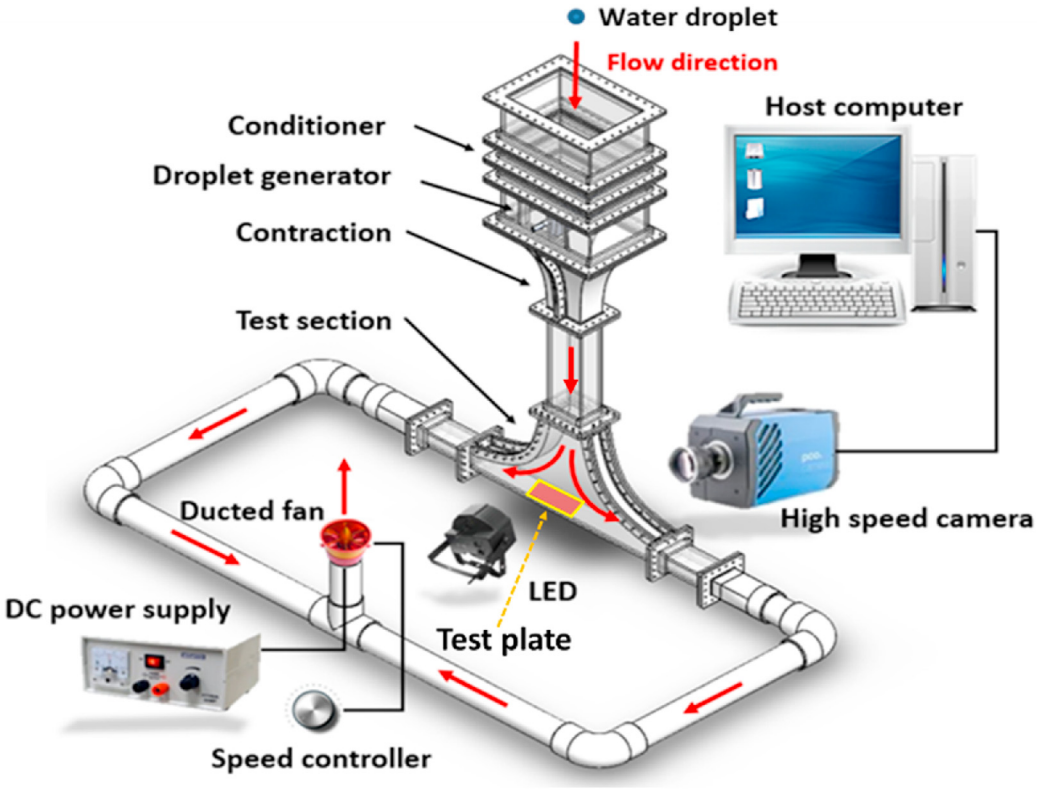

Fig. 6. Experimental setup used to study effects of the SLIPS on droplet impacting dynamic.

generator with a diameter of 3.0 ± 0.1 mm were accelerated up to 10.0 m/s before impinging onto the test plate mounted at the bottom of the vertical wind tunnel. The corresponding Weber number of the impinging droplets would be up to 4000 (i.e., $We \approx 4000$). While a LED spotlight was used to provide light illumination, a high-speed imaging system (i.e., DiMax, PCO) with a macro-lens (50 mm Nikkor 1.8D, Nikon) was used to record the dynamic impacting process of the water droplets. The frame rate for the image acquisition was set at 10,000 Hz, and at least 10,000 frames of snapshot images were recorded for each test cases.

Fig. 7 shows typical acquired snapshot images to reveal the dynamic impacting process of water droplets on the SLIPS coated test plate in comparison to that on the uncoated test plate at the relatively high Webber number of $We \approx 4000$. It can be seen clearly that, upon droplet impacting onto the uncoated test plate, while a portion of the impinged water mass was found to be splashing out from the test surface to generate many tiny "satellite" droplets along the rim of the outspreading ring, majority of the impacted water mass was found to remain on the uncoated test surface to form a thin water film spreading outward. After reaching its maximum diameter at the time instant of $t \approx 2.5$ m s, the impacted water mass was then found to undergo a receding process with the water flowing back toward the impinging center. Corresponding to the hydrophilic nature of the uncoated test plate, the footage of the impacted water droplet (i.e., the size of the wetted area) on the uncoated test plate was found to be almost unchanged during the receding process. After several cycles of the spreading-and-receding process, the impacted water was found to reach a static state and settle down eventually to form a "pancake-like" water film, as shown clearly on the left side of Fig. 7.

As revealed clearly from the snapshot images given on the right side of Fig. 7, upon droplet impinging onto the SLIPS coated test surface, a very similar splashing and expending phenomena were also observed at the initial stage of the droplet impinging process (i.e., $t < 1.0$ m s). However, due to the hydrophobic nature of the SLIPS (i.e., $\theta_{static} \approx 110^{\circ}$ and $CAH \approx 7^{\circ}$), while more obvious splashing were observed, the maximum spreading diameter of the impacted water droplet on the SLIPS coated test plate was found to be about 25% smaller than that over the uncoated test plate. Unlike that on the uncoated test plate, the receding process of the impacted water droplet on the SLIPS coated surface was found to accompany by an obvious breaking up of the inward-receding ring into many tiny water droplets. The tiny droplets generated during the receding process were found to coalesce and bounce off from the test surface, resulting in less impacted water remaining on the SLIPS coated test surface. Furthermore, unlike that of forming a large "pancake-like" water film on the uncoated test plate, the impacted water droplet was found to break into many smaller droplets eventually on the SLIPS coated test surface. As a result, the total wetted area (i.e., the contacting area between the impact water and the test surface) on the SLIPS coated surface was found to become much smaller, in comparison to that over the uncoated test plate.

In summary, the experimental results clearly reveal that, the impinging dynamics of water droplets on the SLIPS coated surface were found to be significantly different from those on the uncoated test surface. After water droplets impacting onto the test plates, while the total wetted area of the impacted water droplet on the SLIPS coated surface was found to become much smaller in comparison to that over the uncoated test surface, the total water mass remaining on the SLIPS coated surface was also found to become less due to the more readily splashing and bouncing of the impacting water droplets on the hydrophobic SLIPS coated surface. The smaller wetted area and less impacted water mass remaining on the SLIPS coated test surface would imply less ice accretion on the SLIPS coated test surface when the droplet impacting process

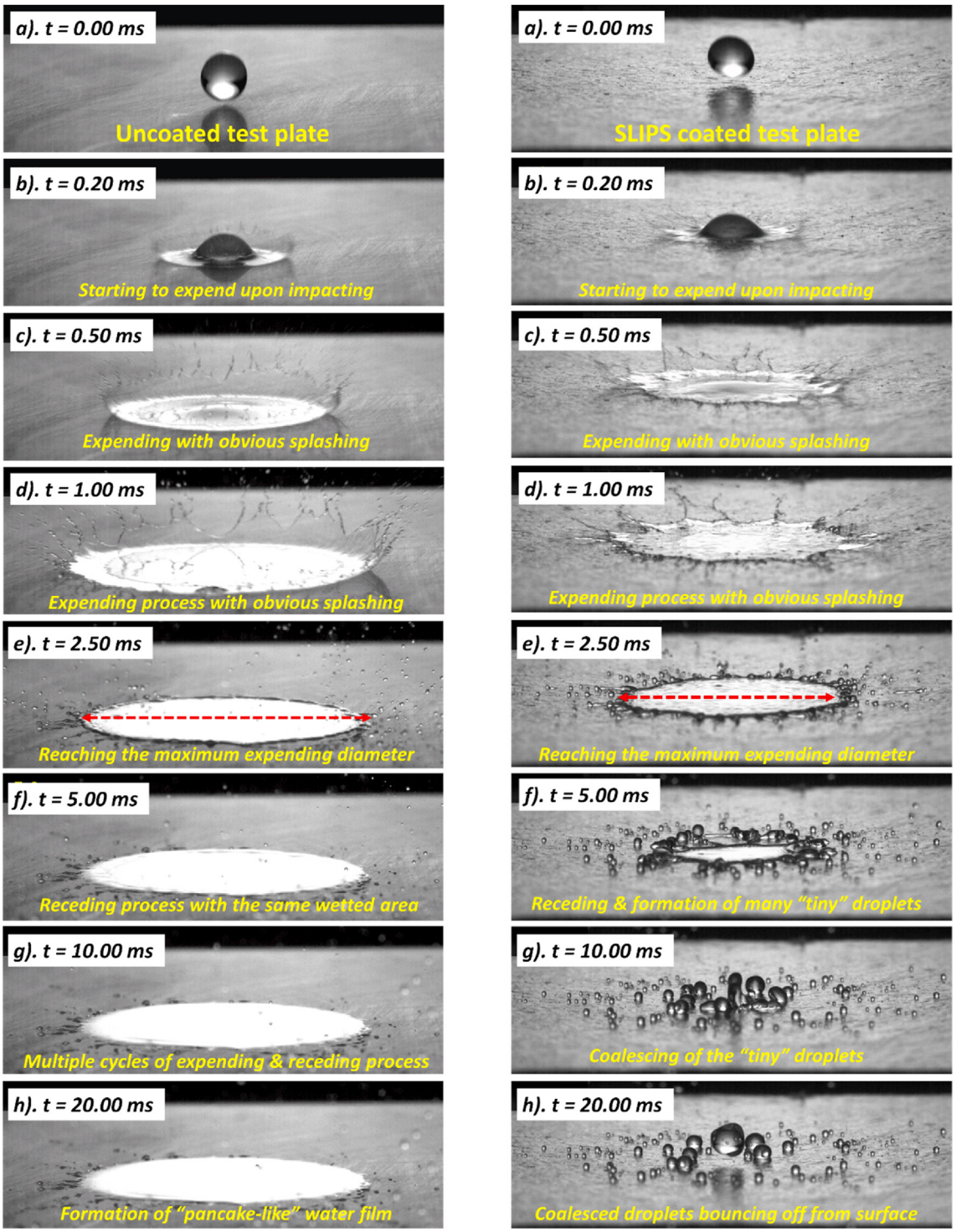

Fig. 7. Snapshot images to reveal the dynamic impacting process of water droplets onto the uncoated and the SLIPS coated test plates.

occurs under an icing condition. Furthermore, due to the much smaller CAH value on the SLIPS coated surface (i.e., CAH $\approx 7^{\circ}$), the water droplets remaining on the SLIPS coated surface after the droplet impingement would also be much more readily to roll off when a shear force is applied to them. For wind turbine icing scenario, due to the existence of shear forces exerted by the incoming airflow around turbine blades, the impacted water droplets on the SLIPS coated blade surfaces would be more easily blown away by the incoming airflow, in comparison to those on the uncoated blade surfaces. This will also result in less ice accretion on the SLIPS coated blade surfaces, which was confirmed by the results of the impact icing experiments to be described in the next section.

3.2. Icing tunnel testing to study the effects of the SLIPS on impact icing process

In the present study, an experimental study was also performed to evaluate the effectiveness of using the SLIPS to suppress impact

icing process over the surface of a wind turbine blade model by leveraging the Icing Research Tunnel of Iowa State University (i.e., ISU-IRT). As shown in schematically Fig. 8, ISU-IRT is a research-grade, multi-functional icing wind tunnel with a test section of 2.0 m in length × 0.4 m in width × 0.4 m in height and four transparent side walls. ISU-IRT was equipped with a 30-hp fan/motor unit (Baldor™) to drive airflow circling inside ISU-IRT with a maximum wind speed up to 60 m/s in the test section. The tunnel is refrigerated via a heat exchanger, which is chilled by a 40-hp compressor (Vilter™), to cool the airflow inside ISU-IRT down to - 25 °C. An array of 8 pneumatic atomizing spray nozzles (Spraying Systems Co., 1/8 NPT-SU11) along with pressure regulators were installed at the entrance of the contraction section of ISU-IRT to inject micro-sized water droplets (i.e., MVD≈ ~20 μm) into the airflow. The flow rate of the de-ionized (DI) water injected into the tunnel was measured by using a digital flow meter (Omega, FLR-1605A). By manipulating the pressure regulators on the air and water supply pipelines of the water spray system, the liquid water content (*LWC*) in the ISU-IRT is adjustable (i.e., ranging from 0.1 g/m^3 to 5.0 g/m^3). In summary, ISU-IRT can be used to simulate various atmospheric icing phenomena over a wide range of icing conditions (i.e., from dry *rime* to extremely wet *glaze* ice conditions).

A wind turbine blade model with DU91-W2-250 airfoil profile in the cross section was manufactured for the impact icing experiments. As shown schematically in Fig. 8, DU91-W2-250 airfoil, which is a cambered airfoil with a blunt leading edge and a maximum thickness of 25% chord length, is well known for its favorable aerodynamic performance and strong structural strength. DU91-W2-250 airfoil profile has been widely used as midspan and outboard airfoil geometry for wind turbine blades of various scales [21,22]. It should be noted that, since modern wind turbines are usually made of polymer-composite materials, the turbine blade model used for the impact ice accretion experiments is also made of a polymer-composite material and has very similar surface properties (i.e., wettability and thermal conductivity) as those of utility-scaled wind turbines. Before applying the SLIPS, the surface of the polymer-composite-based test model was found to be hydrophilic with the static CA $\theta_{static} \approx 65°$ and CAH $\approx 60°$, as listed in Table 1. As shown schematically in Fig. 8, while a high-power LED light unit (RPS Studio Light, Model RS-5620) was used to provide low-flicker illumination during the icing experiments, a high-speed imaging system (PCO - Dimax™ camera with 2000 pixel by 2000 pixel and frame rate of up to 10,000 frames per second) was used to acquire ice accretion images over the surface of the turbine blade model before and after being coated with the SLIPS.

Before performing impact ice accretion experiments, ISU-IRT was operated at a pre-scribed frozen-cold temperature level (e.g., $T_\infty = -5$ °C for the present study) for at least 20 min under a dry testing condition (i.e., without turning on the water spray system) to ensure the ISU-IRT reaching a thermal steady state. After switching on the spray system, supper-cooled water droplets carried by the frozen-cold airflow would impinge onto the surface of the test model (i.e., mainly within the direct impact zone near the airfoil leading edge [53]) to start ice accretion process.

As aforementioned, in comparison to rime ice accretion (i.e., usually occurs at much colder temperatures of $T_\infty < -10$ °C), glaze ice accretion on wind turbine blades (i.e., usually occurs at relatively warmer temperatures of $T_\infty > -10$ °C) was found to be more problematic, and could degrade the aerodynamic performance of turbine blades more significantly, thereby, resulting in a more dramatic power production reduction for the wind turbines [9,54]. Furthermore, more serious ice accretion were usually found to take place in the outbound regions of turbine blades [5]. Therefore, the effectiveness of using SLIPS to mitigate glaze ice accretion on turbine blades is the focus of the present study. Following up the work

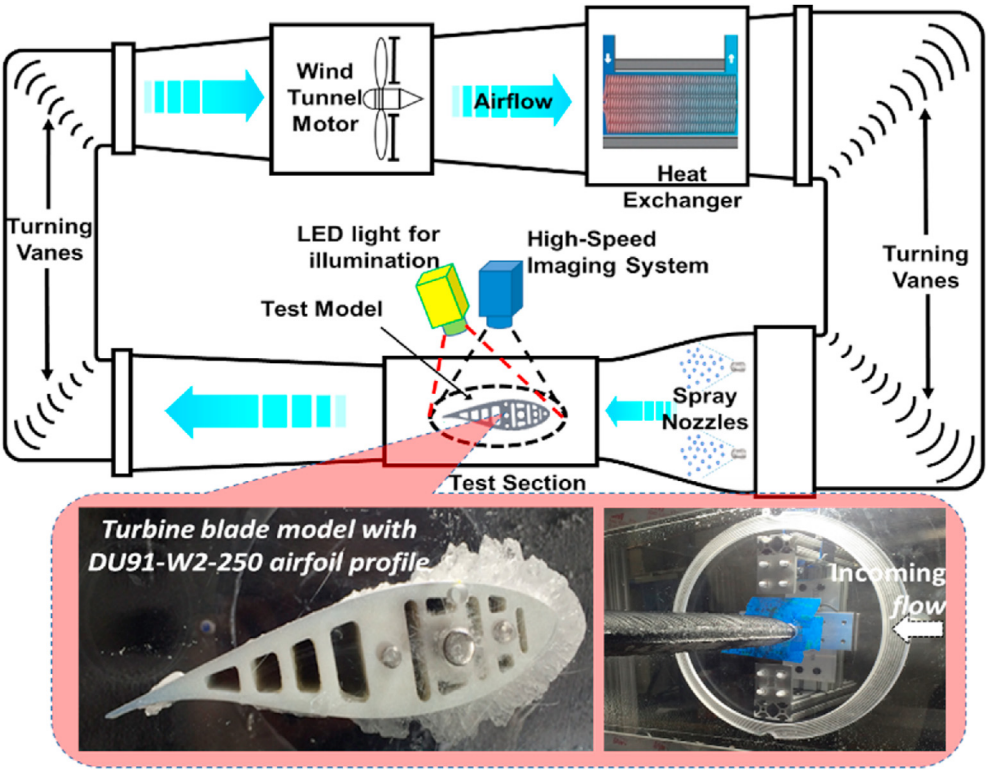

Fig. 8. Schematics of ISU-IRT used to study impact ice accretion process.

of Waldman and Hu [45], in order to generate a typical glaze icing condition in ISU-IRT for the present study, the operation parameters of ISU-IRT were set as the airflow speed of $V_\infty = 40$ m/s; airflow temperature of $T_\infty = -5$ °C; and the liquid water content (LWC) level in the airflow being $LWC = 1.2$ g/m^3.

Fig. 9 shows typical snapshot images to reveal the dynamic ice accretion process over the upper surface of the turbine blade model as a function of the ice accretion time. The effectiveness of the SLIPS to suppress impact ice accretion over the surface of the turbine blade model was reveal clearly based on the side-by-side comparison of the acquired snapshot images for the test cases before and after applying the SLIPS to coat the test model. As shown clearly in Fig. 9(a), for the test case with uncoated test model, upon impacting of super-cooled water droplets carried by the frozen-cold incoming airflow, ice was found to accrete very rapidly on the surface of the test model, mainly within the direct impinging zone of the supercooled water droplets near the airfoil leading edge (LE) [53]. The ice accretion process on the uncoated turbine blade model was found to be a typical glaze ice accretion process with obvious surface water runback and formation of transparent, glassy ice structures over the airfoil surface, as expected.

As shown clearly in Fig. 9(b), after applying the SLIPS to coat/cover the turbine blade model, in addition to having much less ice accretion in the region near the airfoil leading edge (i.e., within the direct impinging zone of the supercooled water droplets), no runback water or ice accretion could be observed on the SLIPS coated turbine surface. The much less ice accretion on the SLIPS coated test model is believed to be caused by following reasons: As revealed clearly from the results of the droplet impacting experiments given in Fig. 7, upon impingement of the same amount of supercooled water droplets, the more readily bouncing and rolling off of the impacted water droplets from the SLIPS coated surface would result in much less water accumulation on the blade surface. As a result, the total amount of the water mass that can be frozen into ice over the SLIPS coated blade surface would become much smaller, in compassion to the case with uncoated test model. Therefore, much less ice accretion was found in the region near the airfoil leading edge for the SLIPS coated blade model. Furthermore, under the glaze icing condition, since only a portion of the impacted water mass would be frozen into ice immediately upon impacting, the remaining unfrozen water would run back along the airfoil surface as driven by the boundary layer airflow. Due to the much more slippery nature of the SLIPS coated surface (i.e., CAH $\approx 7°$) than that on the uncoated hydrophilic surface (i.e., CAH $\approx 60°$ as shown in Table 1), the runback speed of the water droplets/rivulets would be much faster over the SLIPS coated blade surface. Thus, the runback water would roll off much faster, and shed away from the SLIPS coated blade surface eventually before being frozen into ice. Therefore, no runback ice accretion was found over the SLIPS coated blade surface, as shown in Fig. 9. Even for the case with ice having already been accreted on the blade surface, since the ice adhesion strength over the SLIPS coated surface is very small (i.e., $\tau_{ice} \approx 35$ kPa, which is only about 2.5% of that on the uncoated surface), the strong shear forces exerted by the airflow around the airfoil surface would be more readily to sweep the accreted ice away from the SLIPS coated blade surface. This would also contribute to the much less ice accretion on the SLIPS coated surface, as revealed clearly in Fig. 9.

It should also be noted that, even though the total amount of the ice accretion over the SLIPS coated blade surface were found to become much less in comparison to that on the uncoated blade surface, ice structures were still found to accrete in the region near the blade leading edge, especially in the vicinity of the airfoil stagnation line. This highlights one of the major challenges facing by the hydro-/ice-phobic coating strategies for impact icing mitigation. While the hydro-/ice-phobic coatings, including the SLIPS used in the present study, can effectively reduce the adhesion forces between the impacted water and/or accreted ice and blade surface, they still rely on aerodynamic forces acting tangentially to the blade surface to remove the accumulated water/ice. Such approaches would break down at the airfoil stagnation line because the aerodynamic forces near the airfoil stagnation line would be very small or vanish completely. Further exacerbating the problem is that the water collection efficiency reaches its maximum at the

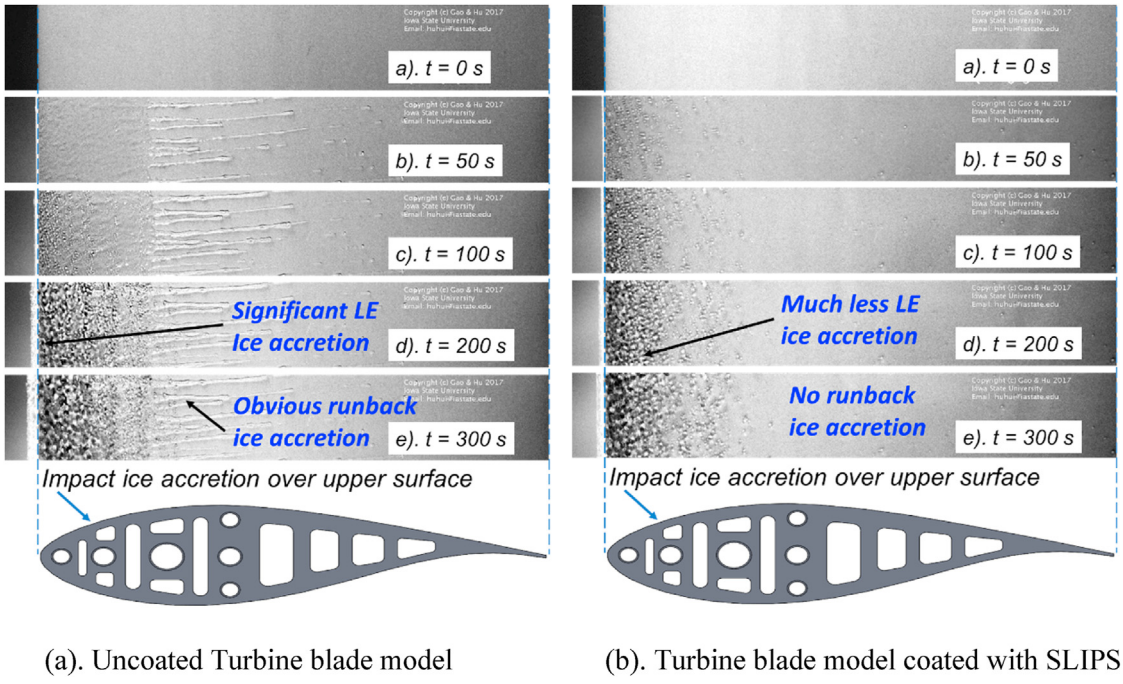

Fig. 9. Typical snapshot images to reveal the dynamic ice accretion process over the surface of the turbine blade models before and after coated with SLIPS.

stagnation line. Once ice started to accrete along the stagnation line, the next groups of the super-cooled water droplets carried by the incoming airflow would impact directly onto the surface of the accreted ice, instead of the SLIPS coated blade surface. Therefore, more and more ice structures were found to accrete in the region near the airfoil leading edge as the ice accretion time increases. To remove ice accretion from the region near the airfoil stagnation line, this is usually accomplished by heating the airfoil surface with electric-thermal heaters or hot air bleeding systems to brutally melt out the ice accreted near the airfoil leading edge.

To prevent/remove ice accretion over entire turbine blade surface, we suggested a novel hybrid anti-/de-icing strategy, which integrate the icephobic SLIPS with the minimized surface heating near airfoil leading-edge (i.e., LE heating). To demonstrate the outstanding performance of the hybrid anti-/de-icing strategy, an experiment study was also conducted to compare different anti-/de-icing strategies, i.e., 1) the baseline case with neither LE heating nor the SLIPS; 2) a passive method with the SLIPS only, but no LE heating; 3) an active approach with LE heating only, but no the SLIPS; and 4) the hybrid strategy to integrate the SLIPS with minimized LE heating. Fig. 10 gives a side-by-side comparison of the 4 test cases after 10 min of the impact icing experiments under the same glaze icing conditions of $V_\infty = 40$ m/s; $T_\infty = -5$ °C; and $LWC = 1.2$ g/m^3. It can be clearly seen that, for the baseline case (i.e., uncoated blade surface and no LE heating), while a large amount of ice structures were found to accrete in the region near the airfoil leading edge, obvious runback water/ice structures were also observed at further downstream locations, as shown clearly in Fig. 10(a). It was revealed clearly from Fig. 10(b) that, after applying the SLIPS to coat/cover the turbine blade surface, the aerodynamic forces exerted by the airflow above the airfoil surface were found to sweep away the impinged water droplets/accreted ice structures from most of the airfoil surface, except in the vicinity of the stagnation line due to the high impinging pressure and extremely small aerodynamic forces at those locations. Fig. 10(c) shows clearly that, after turning on the heating element flush mounted around the airfoil leading-edge, the ice structures accreted in the region near the airfoil leading-edge were found to be eliminated effectively. However, the surface water from the melt ice was found to simply run back, and re-freeze into runback ice at further downstream locations. As shown clearly in Fig. 10(d), by integrating the SLIPS with minimized LE heating, the hybrid strategy was found to be able to keep the entire blade surface completely free of ice (i.e., no ice accretion both in the region near the blade leading edge and the further downstream region) during the whole ice accretion experiment, even though the power input for the novel hybrid anti-/de-icing strategy is only ~20% of that required for the conventional surface heating only method (i.e., the test case shown in Fig. 10(c). In summary, the hybrid anti-/de-icing strategy to integrate the SLIPS with minimized LE heating was demonstrated to be very effective to suppress impact ice accretion over turbine blade surfaces. In comparison to the conventional brute-force surface heating methods, the hybrid anti-/de-icing strategy was found to be able to effectively prevent ice accretion over entire surface of the turbine blade model at a much lower power consumption (i.e., up to ~ 90% energy saving) for the anti-/de-icing operation.

3.3. Rain erosion testing to characterize the degradation of SLIPS due to rain erosion effects

The experimental results given above have shown clearly that the SLIPS is very promising to suppress impact ice accretion for wind turbine icing mitigation, especially when integrated with a minimized LE heating to make up a hybrid anti-/de-icing system. Since wind turbines would be exposed to the continuous impingement of super-cooled water droplets for a relatively long time, the durability of SLIPS to resist “rain erosion” effects (i.e., the capability to withstand the damages to the substrate materials or/and performance degradation caused by the continuous impingement of water droplets at high impacting speeds) would be very critical in considering the practical applications of the SLIPS for wind turbine icing mitigation. In the present study, a rain erosion

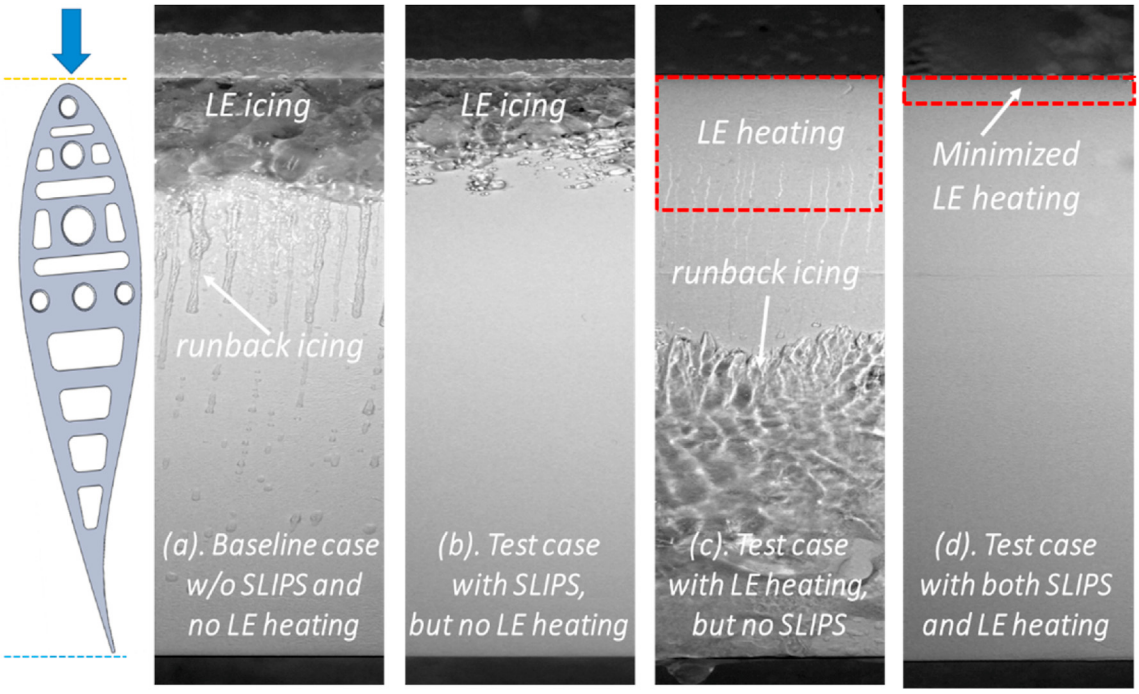

Fig. 10. Comparison of different anti-/de-icing strategies for impact icing mitigation.

testing campaign was also performed to examine the "rain erosion" characteristics of the SLIPS undergoing continuous impingement of water droplets at impacting speeds up to ~90 m/s (i.e., the typical droplet impacting speed in the regions near blade tips of utility-scale wind turbines).

Fig. 11 shows the experimental setup used for the rain erosion testing. A high-thrust electric ducted fan (EDF, JP Hobby) is installed at the inlet to drive airflow into a circular-shaped wind tunnel. By manipulating the power supplied to the ducted fan, the speed of the airflow exhausted from the wind tunnel nozzle ($D_{nozzle} \approx 40$ mm) can be adjusted from 20 m/s to 100 m/s. While a water spray nozzle (BIMV-11002 nozzle) is integrated in the middle section of the wind tunnel, De-Ionized (DI) water is supplied to the spray nozzle to generate micro-sized water droplets (i.e., 10–100 μm in diameter) and inject them into the airflow. By manipulating the water flow rate supplied to the spray nozzle, the liquid water content (*LWC*) levels in the airflow can be changed for different testing conditions. It should also be noted that, while typical *LWC* levels in the airflow for most of the atmospheric icing events (e.g., wind turbine icing phenomena) are in the range of $LWC \approx 0.5–1.0$ g/m^3, the rain erosion test experiments of the present study were designed intentionally with much higher *LWC* levels in the incoming airflow (i.e., $LWC \approx 15–20$ g/m^3) in order to accelerate the degradation of the SLIPS caused by the rain erosion effects.

During the rain erosion experiments, in addition to using a high-speed imaging system to record the dynamic impinging of the water spray flow (i.e., the water droplets carried by the airflow) onto the SLIPS coated test plate under different test conditions (i.e., droplet impacting speed varying from 55–85 m/s for the present study), the variations of the surface wettability and the ice adhesion strengths on the SLIPS coated surface were also characterized quantitatively as a function of the rain testing duration. Fig. 12 gives some typical snapshot images to reveal the rain erosion effects on the SLIPS under the testing condition of $V_\infty = 65$ m/s and $LWC = 15$ g/m^3. As revealed clearly from the acquired image given in Fig. 12(a), very strong light reflection was observed due to the existence of the excess lubricant oil layer on the SLIPS coated test plate before starting the rain erosion experiment. During the rain erosion testing, the impacted water droplets were found to slide away radially from the impingement center of the water spray flow, which were visualized as the radial streak lines in the acquired images given in Fig. 12. Meanwhile, due to the continuous impingement of the water spray flow, the excess lubricant oil on the SLIPS coated test plate was found to be flushed away from the center of the spray impinging zone gradually. As the time of the rain erosion testing increases, corresponding to the thinner and thinner lubricant oil film remaining on the SLIPS coated test plate, the reflected light intensity was found to become weaker and weaker. It should be noted that, even though the excess lubricant oil layer over the surface of the SLIPS coated test plate was almost flushed away completely after 600 s of rain erosion testing, the lubricant oil infused inside the porous layer was found to be still able to keep the test surface very slippery to make the impacted water droplets sliding quickly away from the center of the spray impinging zone, as shown clearly in Fig. 12(f).

In order to reveal the degradation of the SLIPS induced by the rain erosion effects more quantitatively, the droplet advancing CA, $\theta_{adv.}$, receding CA, θ_{rec}, and ice adhesion strength on the SLIPS coated surface after undergoing the rain erosion testing were measured. The rain erosion testing would stop when reaching to pre-selected time durations. Then, the measurements of the contact angles and ice adhesion strength were performed with the same procedures as those described in section 2.2. The rain erosion experiment would be resumed after finishing the contact angle and ice adhesion measurements. Fig. 13 gives the measured advancing and receding CA values as a function of the rain erosion testing duration under different test conditions. It can be seen clearly that, while the droplet advancing CA on the eroded SLIPS surface was found to be almost unchanged (i.e., $\theta_{adv} = 115° \pm 2°$), the receding

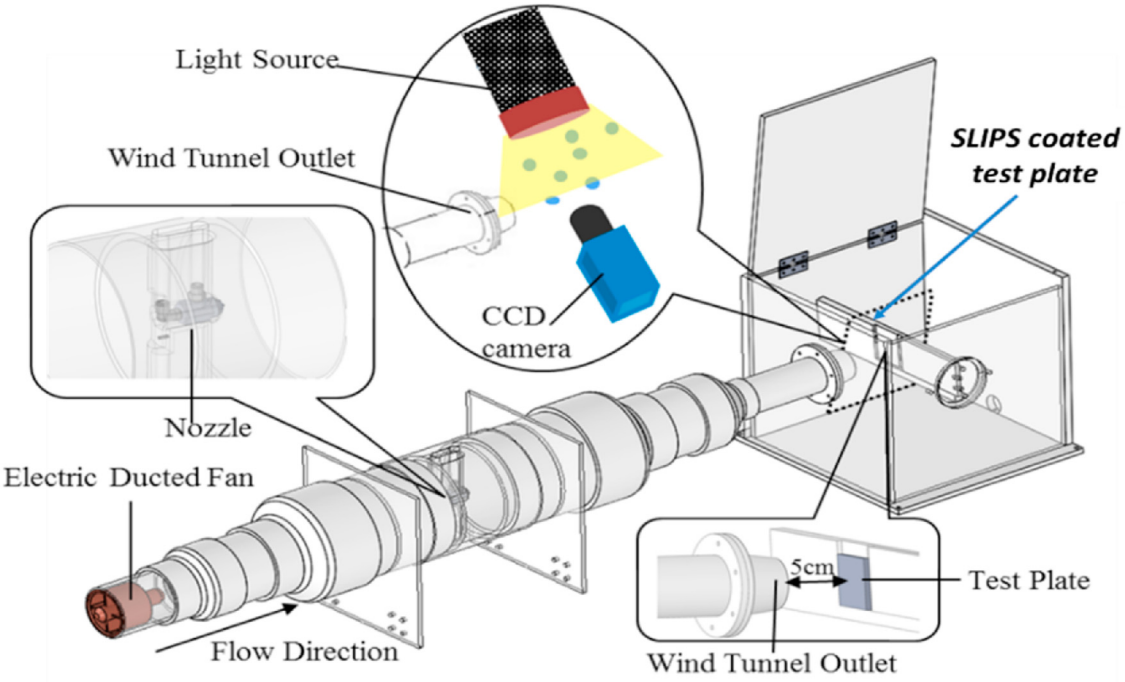

Fig. 11. Experimental setup used to evaluate rain erosion effects on the SLIPS.

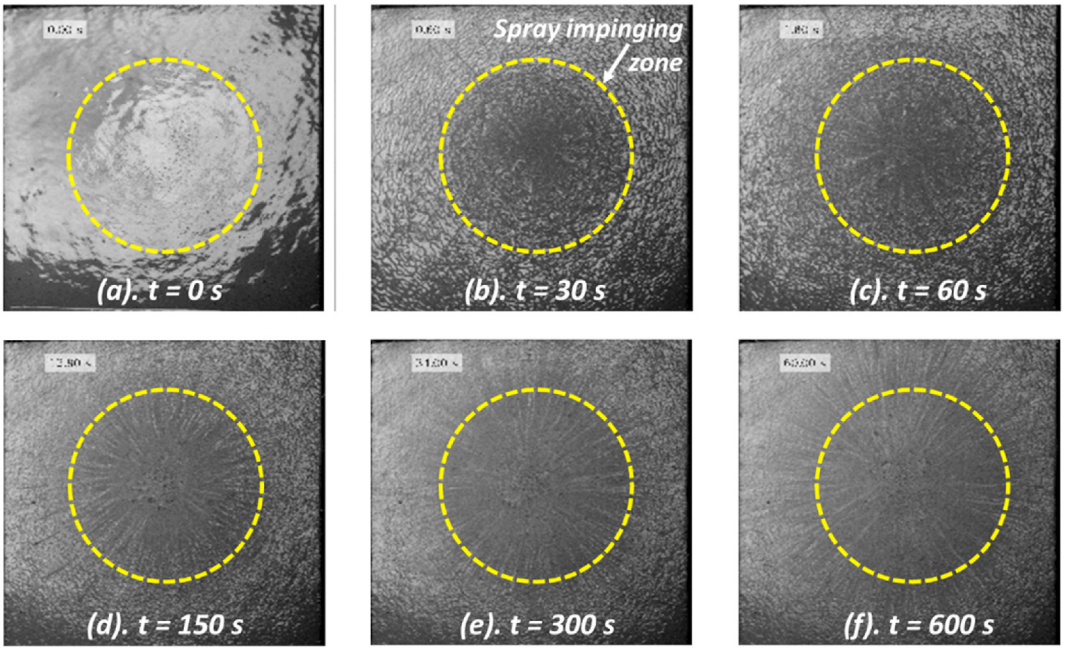

Fig. 12. Snapshot images to reveal the impinging water spray flow on the SLIPS coated plate.

CA was found to decrease monotonically as the duration of the rain erosion testing increases. The relationships between the measured receding CA value and the rain erosion testing duration under different test conditions were found to be fitted well by using exponential functions, which are shown as the dashed curves in Fig. 13.

Based on the measured advancing and receding CA values given in Fig. 13, the corresponding Contact Angle Hysteresis (CAH) values can also be determined. As aforementioned, CAH value is usually used to refer the tendency of a water droplet to bounce or/and roll off the surface. For wind turbine icing scenario, it is highly desirable to make turbine blades having a smaller CAH value so that the impacting water droplets would be more readily to bounce and roll off from the blade surface, resulting in less ice accretion on the blade surface. Based on the measurement data given in Fig. 13, it can be seen clearly that, the CAH value of the SLIPS coated surface would increase rapidly at the initial stage of the rain erosion testing, coordinating well with the rapidly flushing away of the excess lubricant oil from the SLIPS coated surface as visualized in the snapshot images given in Fig. 12. With the lubricant oil remaining on the SLIPS coated test plate becoming thinner and thinner, the CAH value on the eroded SLIPS surface was found to change much more slowly as the duration of the rain erosion testing increases. The corresponding value was found to approach to a constant of

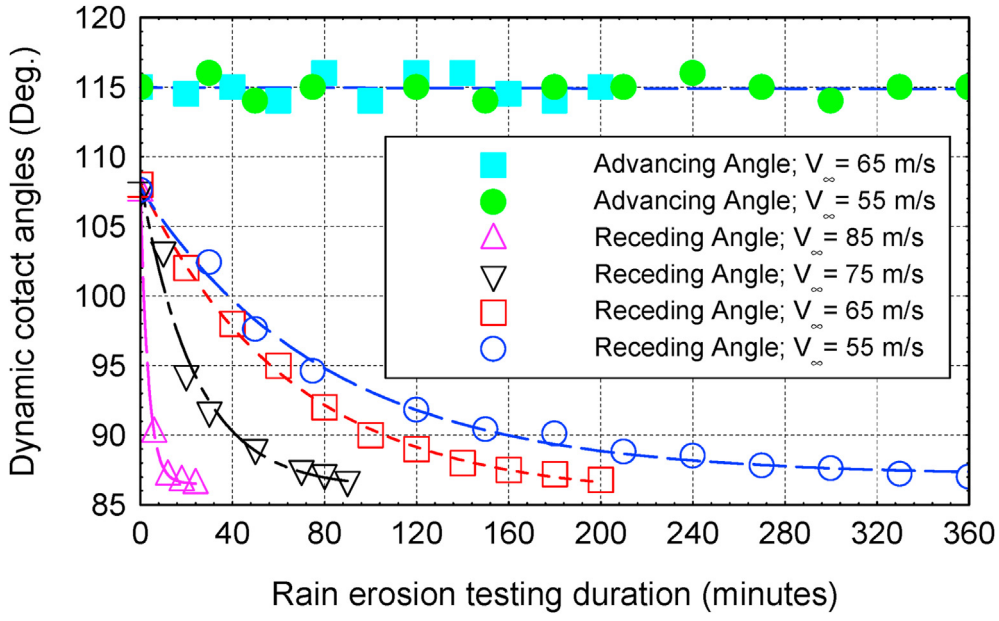

Fig. 13. Variations of the advancing and receding CA values on the SLIPS coated test plate against the rain erosion testing duration.

CAH ≈28° eventually when the excess lubricant oil on the SLIPS coated surface was almost flushed away completely.

While the measurement results obtained under different rain erosion testing conditions were found to show very similar wettability degradation characteristics, the increment of the CAH values due to the rain erosion effects were found to take place much faster for the test cases with higher spray impinging speeds, in comparison to those with lower droplet impacting speeds. More specifically, for the test case with the droplet impacting speed being $V_\infty = 55$ m/s, the CAH value was found to increase from its initial values of $CAH \approx 7°$ to $CAH \approx 28°$ after 360 min of the rain erosion testing. However, after the droplet impacting speed increases to $V_\infty = 85$ m/s, the corresponding CAH value was found to increase to CAH ≈ 28° after only 20 min of the rain erosion testing. It should also be noted that, even though the CAH value on the SLIPS coated surface was found to increase substantially due to the rain erosion efforts, the value of CAH ≈ 28° on the eroded SLIPS was found to be still much smaller than that of the uncoated test plate (i.e., CAH ≈ 60°). It confirms that, even though the lubricant oil on the SLIPS coated test plate was flushed away due to the rain erosion effects, the lubricant oil infused inside the porous substrate was still found to be able to keep the test surface being very slippery.

Fig. 14 gives the measured ice adhesion strengths on the SLIPS coated test plate as a function of the rain erosion testing duration under the testing conditions of $V_\infty = 75$ m/s and $LWC = 13$ g/m^3. It can also be seen clearly that, due to the existence of the excess oil film over the SLIPS, the ice adhesion strength was found to be $\tau_{ice} \approx 35$ kPa before starting the rain erosion testing. Since the excess oil film over the SLIPS was flushed away by the impinging water spray flow, in addition to the surface wettability degradation as shown quantitatively in Fig. 13, the ice adhesion strengths on the SLIPS coated test plate were also found to increase monotonically as the rain erosion testing duration increases. More specifically, after 100 min of the rain erosion test experiment with $V_\infty = 75$ m/s and $LWC = 13$ g/m^3, the ice adhesion strength on the eroded SLIPS was found to increase to $\tau_{ice} \approx 50$ kPa, i.e., about 43% increase in comparison to the initial value of $\tau_{ice} \approx 35$ kPa. It should also be noted that the ice adhesion strength on the eroded SLIPS is still much smaller than that of the uncoated test plate (i.e., $_{ice} \approx 1400$ kPa). The relationship between the ice adhesion strength data and the rain erosion testing duration was also found to be fitted well by using an exponential function, which is shown as the dashed curve given in Fig. 14.

In order to reveal the rain erosion induced damages to the SLIPS more clearly, a comparative study was also conducted by preparing two identical test plates covered with same porous layers (i.e., the same nanofibrous laminated PTFE membranes), but applying lubricant oil of Krytox® 103 to only one of the porous layers. With the water spray impinging onto the test plates under the same conditions of $V_\infty = 75$ m/s and $LWC = 13$ g/m^3, rain erosion experiments were conducted until obvious structural damages to the porous layers were found due to the rain erosion effects. The test case with the dry porous layer (i.e., without applying lubricant oil to the porous layer) is referred as the baseline case for the comparative study.

Fig. 15 gives the snapshot images of the two test plates after undergoing the rain erosion testing. As shown clearly in Fig. 15(a), due to the rain erosion effects, obvious surface damages were found to occur much earlier for the baseline case with “dry” porous layer. The porous layer was found to be torn up by the impinging water spray within less than 10 min. Enlarged views of the eroded test surfaces at selected regions (i.e., indicated by the red circles) were also provided to reveal the rain erosion effects more clearly. It can be seen clearly that, the undamaged surface of the porous layer shown in the window #A (i.e., in the region far away from the impinging center of the water spray flow) was found to have relatively smooth surface textures of the laminated PTFE membrane, as expected. Some fragments of the porous layer on the edge of the impinging water spray flow shown in the window #B were found to be blown away due to the strong shear forces exerted by

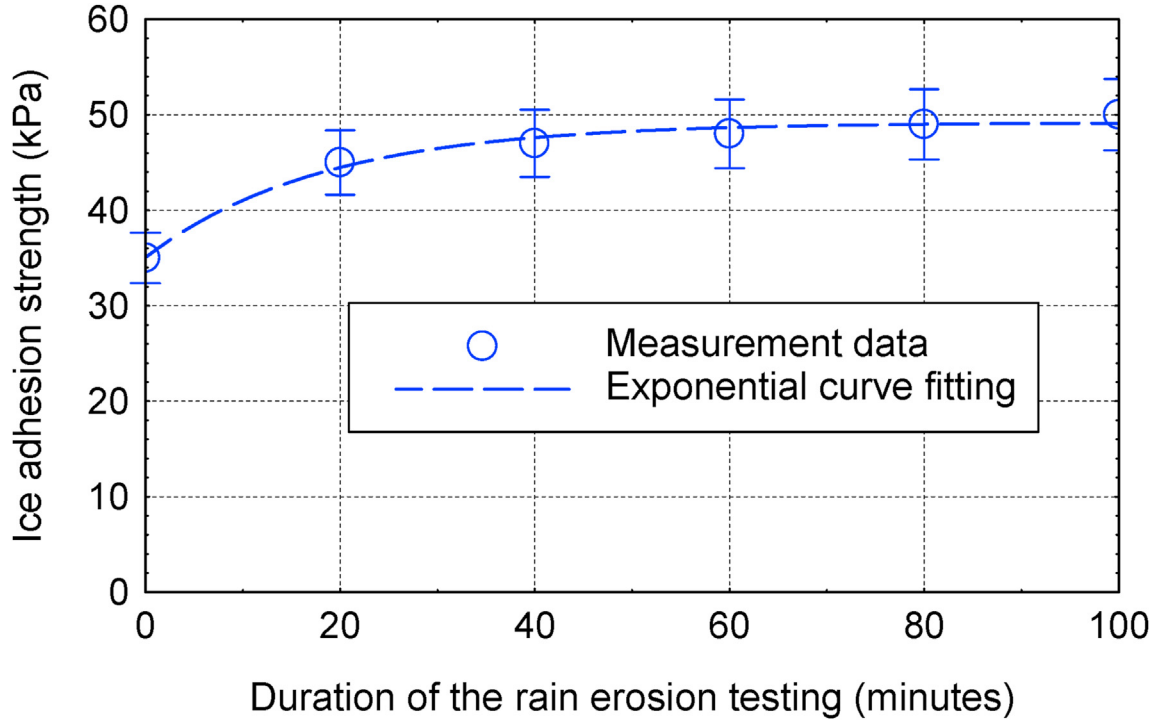

Fig. 14. Measured ice adhesion strength on the SLIPS coated test plate as a function of the rain erosion testing duration.

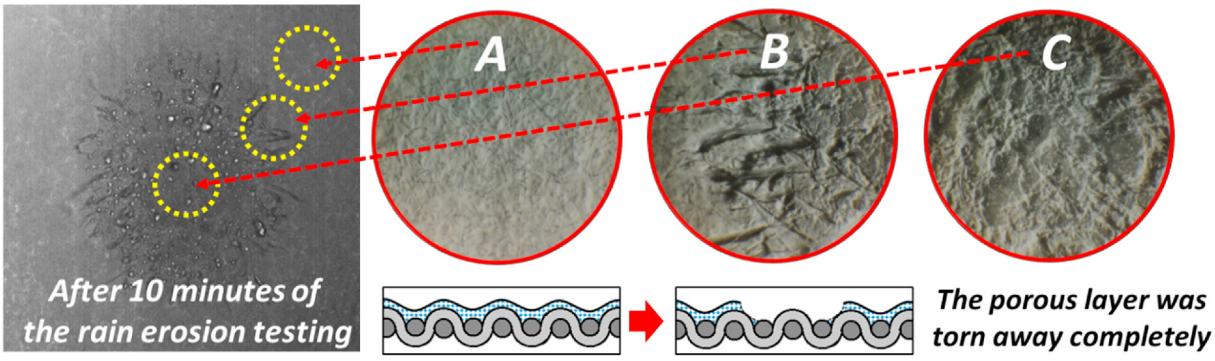

(a). The test case without applying the lubricant oil to the porous layer

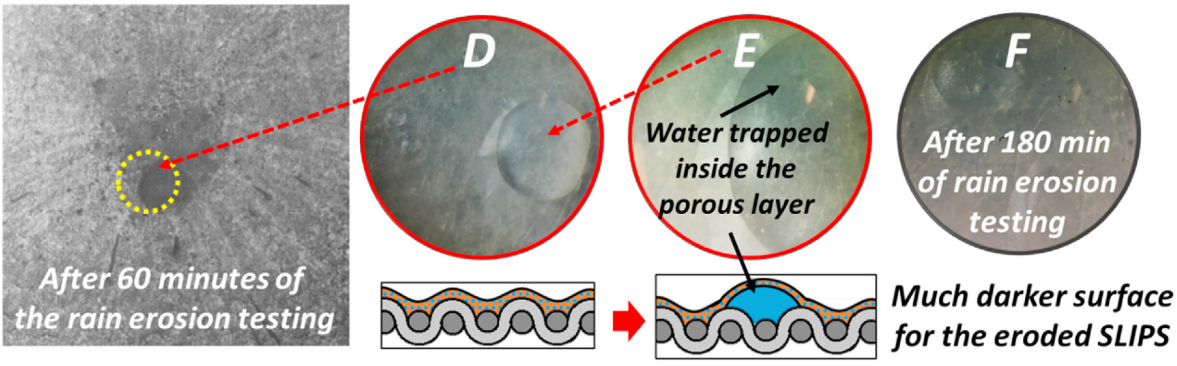

(b). The test case with applying the lubricant oil to infuse into the porous layer

Fig. 15. The damages induced by the rain erosion effects to the test plate before and after infusing the lubricant oil into the porous substrate.

the impinging water spray. As shown clearly in the window #C, surface textures of the porous layer were found to be smashed and teared apart from the substrate completely, due to the much stronger rain erosion effects at the center of the impinging zone of the water spray.

After applying the lubricant oil to infuse into the porous layer to form SLIPS, the PTFE membrane was found to become much more durable to resist the rain erosion, in comparison to the baseline case with "dry" PTFE membrane. However, since the lubricant oil on the surface of the porous layer was flushed away by the impinging water spray, some noticeable damages were found to occur over the SLIPS coated surface after undergoing 60 min of the rain erosion experiment. As shown clearly in Fig. 15(b), the damages induced by the rain erosion were found to be quite different from those of the baseline case with "dry" porous layer. Instead of tearing away the porous layer completely from the test plate, much localized damages were found to take plate on the SLIPS coated test surface. After the depletion of the lubricant oil infused inside the porous layer, the impinging water spray was found to be able to penetrate into the porous layer, and accumulate inside the gaps between the fabrics of the PTFE membrane, as revealed clearly from the zoom-in image of window #D. The penetration of the impacted water into the porous layer can be observed much more clearly from the further enlarged view given in window #E, where both air and water were found to trapped beneath the top surface of the porous layer. As the rain erosion experiment continues, more and more damages were observed on the SLIPS coated test surface. As revealed clearly from the image given in the window #F, due to the aggregation of more and more damaged fabric elements of the PTFE membrane, the eroded SLIPS coated test plate was found to become much darker in color after 180 min of the rain erosion experiment.

Based on the experimental observations described above, the damages to the SLIPS induced by the rain erosion effects can be summarized into several stages, which are shown schematically in Fig. 16. For the SLIPS, the lubricant oil was found to play an essential role to maintain its functionality. As shown in Fig. 16(a), the existence of the excess lubricant oil above the porous layer was found to make the SLIPS coated surface very slippery (i.e., CAH $\approx 7^{\circ}$) with ultra-low ice adhesion strength (i.e., $\tau_{ice} \approx 35$ kPa, which is about 2 orders of magnitude smaller than that on the uncoated surface). Upon impinging of the water spray flow, the extra lubricant oil over the porous layer was found to be flushed away as driven by the impinging water spray. Corresponding to the thinner and thinner lubricant oil film over the porous layer, the surface wettability was found to degrade gradually (i.e., in the term of CAH value to quantify the surface slipperiness) accompanied with a monotonic increment of the ice adhesion strength over the SLIPS coated surface. As shown schematically in Fig. 16(b), even after the extra lubricant oil over the porous layer was flushed away completely, a good water/ice repellency was still found to be achieved by the lubricant oil infused inside the nanoscopic pores of the porous layer (i.e., the CAH $\approx 28^{\circ}$ and $\tau_{ice} \approx 50$ kPa). It should be noted that, since the performance degradation is mainly caused by the depletion of the lubricant oil, the SLIPS could easily recover to its original state when the lubricant oil is refilled at this stage.

As shown in Fig. 16(c), when the SLIPS coated surface is exposed to further rain erosion testing without refilling the lubricant oil, more hazardous oil depletion would take plate to dry out the

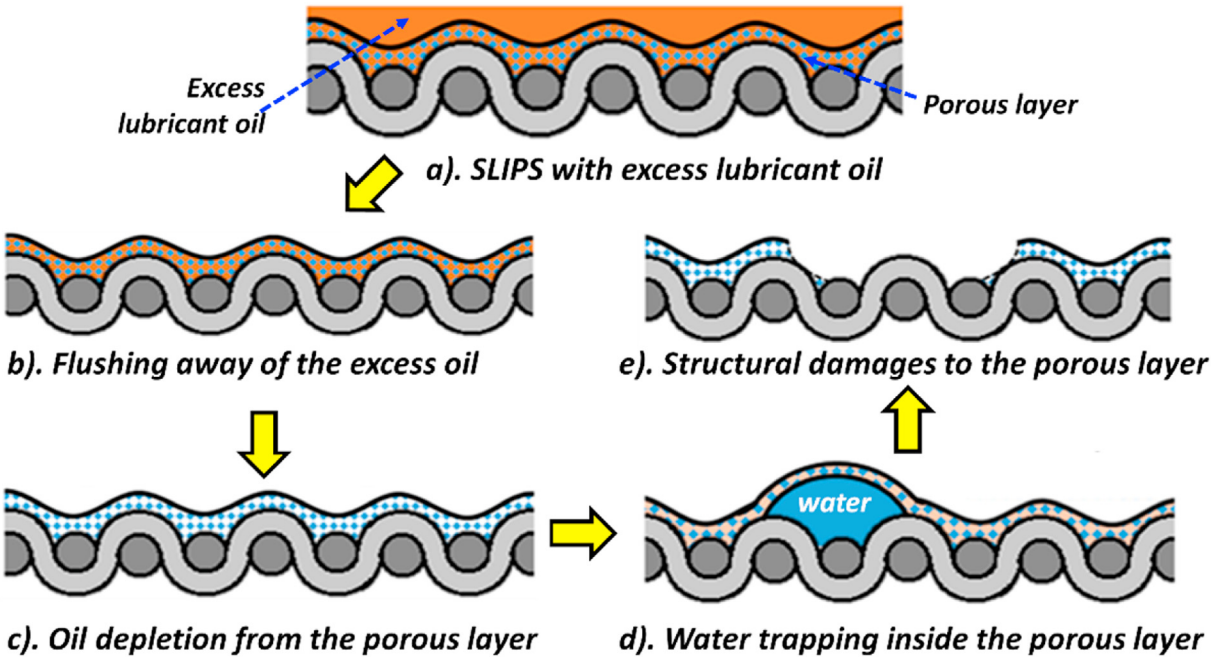

Fig. 16. The schematic of the "rain erosion" damages to the SLIPS.

lubricant oil infused inside the porous layer. Corresponding to the further depletion of the lubricant oil, the impacting water spray would be able to penetrate inside the porous layer. As a result, the impacted water and air were found to be trapped beneath the top surface of the porous layer to form water/air bulges protruding out from the porous layer, as shown schematically in Fig. 16(d). As the rain erosion testing continues, the water/air bulges trapped inside the porous layer were found to grow bigger and bigger, causing the breakdown of the porous layer, as shown in Fig. 16(e). This would eventually make the porous layer being either detached or entirely removed from the substrate. Such structural damages induced by the rain erosion effects are unrecoverable.

4. Conclusions

An experimental study was conducted to explore/demonstrate the feasibility of using a Slippery-Liquid-Infused-Porous-Surface (SLIPS) with ultra-low ice adhesion strengths for wind turbine icing mitigation. The SLIPS was prepared by infusing a lubricant fluid of DuPont's Krytox® 103 into a porous layer of nanofibrous Polytetrafluoroethylene (PTFE) membrane, which can stick firmly to the surfaces of test models. The impinging dynamics of water droplets onto a SLIPS coated test plate at a high Weber number of $We \approx 4000$ (i.e., in the range pertinent to wind turbine icing) was examined, in comparison to that on an uncoated test plate. By leveraging the Icing Research Tunnel of Iowa State University (i.e., ISU-IRT), an experimental campaign was also conducted to evaluate the effectiveness of using the SLIPS to suppress dynamic impact icing process over the surface of a turbine blade model.

Based on the side-by-side comparison of the dynamic impact ice accretion process over the surface of a SLIPS coated turbine blade model to that of uncoated blade surface, it was demonstrated clearly that impact icing process would be suppressed greatly by applying the SLIPS to coat the turbine blade model. The much less ice accretion over the SLIPS coated blade surface can be explained with following three reasons: 1). Upon impacting of the super-cooled water droplets carried by the incoming airflow, the much slippery SLIPS would make the impacted water droplets more readily to bounce and roll off from the surface of the turbine blade model. This will result in much less impacted water mass remaining on the blade surface, thereby, substantially reduce the ice accretion on the surface of the SLIPS coated blade model. 2). As driven by the incoming airflow around the blade surface, the much smaller droplet contact angle hysteresis (CAH) value on the SLIPS coated blade surface (i.e., CAH $\approx 7^{\circ}$) would enable the unfrozen water to run back much faster along the turbine blade surface, in comparison to those on the uncoated, hydrophilic blade surface (i.e., CAH $\approx 60^{\circ}$). As a result, the unfrozen water would shed off much more quickly from the blade surface before being frozen into ice, thereby, eliminating the formation of runback ice structures over the SLIPS coated blade surface. (3) The ultra-low ice adhesion strength on the SLIPS (i.e., about 2 orders of magnitude smaller than that on the uncoated blade surface) would enable the aerodynamic shear forces exerted by the incoming airflow more likely to sweep away the ice structures accreted on the SLIPS coated blade surface, which would also contribute to the much less ice accretion over the SLIPS coated blade surface.

While SLIPS was demonstrated to be effective to mitigate the impact ice accretion in the regions where strong aerodynamic shear forces are exerted, obvious ice accretion was still found to take place in the region around the leading edge of the turbine blade model (i.e., in the vicinity of the stagnation line) where the aerodynamic shear stresses are at their minimum. A novel hybrid anti-/de-icing strategy is suggested by integrating the SLIPS with a minimized surface heating in the region near the blade leading-edge to prevent/remove impact ice accretion over entire turbine blade surface. The hybrid anti-/de-icing strategy was demonstrated to be very effective in preventing ice accretion over the entire surface of the turbine blade model at a much lower power consumption than conventional brute-force surface heating methods.

In considering the practical applications of SLIPS for wind turbine icing mitigation, an experimental investigation was also performed to examine the durability of the SLIPS to resist "rain erosion" effects, i.e., to evaluate the capability of the SLIPS to

prevent the wearing away of substrate materials or/and depletion of infused lubricant liquid by continuous impingement of water droplets at high impacting speeds up to ~90 m/s (i.e., the droplet impinging speed in the outbound regions near the blade tips of utility-scale wind turbines). The degradation characteristics of the surface wettability (i.e., in term of the contact angle hysteresis (CAH) values of water droplets to quantify the slipperiness of the SLIPS) and the ice adhesion strengths on the SLIPS coated test plate were quantified as a function of the duration of the rain erosion experiment under different testing conditions. It was found that the, while both the CAH value and the ice adhesion strength on the eroded SLIPS were found to increase monotonically with the increasing time of the rain erosion experiment, the performance degradation was found to occur much faster for the test cases with higher droplet impacting speeds. The surface wettability degradation and the ice adhesion strength increment on the eroded SLIPS surfaces were found to correlate well with the damage patterns induced by the rain erosion effects. It was found that, after the lubricant oil infused inside the porous layer being flushed away due to the continuous impingement of the water spray, the impacted water droplets would be able to penetrate into the porous layer to form water bulges protruding out from the porous layer, which would eventually cause the breakdown of the porous layer and detach of the SLIPS from the substrate.

It should be noted that, while extensive studies have been conducted on SLIPS in recent years, the present study is believed to be the first to explore/demonstrate the feasibility of using SLIPS to suppress the impact ice accretion process (i.e., due to the dynamic collision of water droplets at high impacting speed of ~100 m/s) on wind turbine blade surfaces for wind turbine icing mitigation. It is also belived to be the first comprehensive study to examine the rain erosion characteristics of SLIPS coated surface due to the continuous impingement of water droplets at high impacting speeds pertinent to wind turbine icing phenomena. While the present study has revealed that SLIPS is very promising to suppress impact ice accretion process over the surfaces of wind turbine blades and the hybrid anti-/de-icing strategy (i.e., to integrate the SLIPS with minimized surface heating near blade leading-edge) is very effective to prevent ice accretion over the entire surfaces of the turbine blades, the experimental study was performed in a simplified laboratory setting with a 2-D turbine blade section model exposed in straight-line winds and under idealized testing conditions. Much more researches are needed to improve the Technology Readiness Level (TRL) of the hybrid anti-/de-icing strategy in order to develop effective and robust SLIPS-based anti-/de-icing systems, and to implement them to wind turbines siting in wind farms with complex terrains and under violent natural icing conditions. While the research program is ongoing, some of the research topics to be explored in the future will include, but are not limited to, 1). To conduct a comparative study to evaluate the effects of SLIPS on the aerodynamic performance (i.e., lift and drag forces) of turbine blade models with the test models with and without applying the SLIPS to coat the surface of the blades models; 2). To carry out more extensive parametric studies to explore/optimize design paradigms of the hybrid anti-/de-cing strategies; 3). To conduct a pilot field testing campaign to implement the novel SLIPS-based anti-/de-icing systems (e.g., the hybrid anti-/de-icing strategy to integrate the SLIPS with minimized surface heating near blade leading-edge) on utility-scaled wind turbines for better icing protection; and 4). To perform a comprehensive techno-economic (TA) analysis to evaluate the economic benefits of using the hybrid anti-/de-icing strategy (i.e., to integrate the SLIPS with minimized surface heating near blade leading-edge) in comparison to conventional brute-force surface heating methods by taking all the energy expenditures and maintenance costs into account. The ultimate goal of the research program is to develop a new class of effective, robust and low-power, SLIPS-based anti-/de-icing strategies tailored specifically for wind turbine icing mitigation.

CRediT authorship contribution statement

Liqun Ma: Data curation, contributed significantly to performing experiments and collecting measurement data. **Zichen Zhang:** Data curation, contributed significantly to performing experiments and collecting measurement data. **Linyue Gao:** Data curation, contributed significantly to performing experiments and collecting measurement data. **Yang Liu:** Data curation, Formal analysis, contributed to the experimental data analysis and graph preparation. **Hui Hu:** Writing - original draft, contributed to the formulation of the research objectives and paper writing.

Declaration of competing interest

The authors declare that they do not have any known competing interests that could have appeared to influence the work reported in this paper.

Acknowledgments

The authors would like to thank Dr. Tak-Sing Wong of Pennsylvania State University for help in preparing the SLIPS. The research work is partially supported by Iowa Energy Center for Wind Turbine Icing Study under the IEC Competitive Grant # 312350, and National Science Foundation (NSF) under the grant numbers of OISE-1826978, CMMI-1824840 and CBET-1916380.

Appendix A. Supplementary data

Supplementary data to this article can be found online at https://doi.org/10.1016/j.renene.2020.10.013.

References

[1] R. Wiser, E. Lantz, T. Mai, J. Zayas, E. DeMeo, E. Eugeni, J. Lin-Powers, R. Tusing, Wind vision: a new era for wind power in the United States, Electr. J. 28 (2015) 120–132, https://doi.org/10.1016/j.tej.2015.09.016.
[2] F. Lamraoui, G. Fortin, R. Benoit, J. Perron, C. Masson, Atmospheric icing impact on wind turbine production, Cold Reg. Sci. Technol. 100 (2014) 36–49, https://doi.org/10.1016/j.coldregions.2013.12.008.
[3] L. Gao, Y. Liu, W. Zhou, H. Hu, An experimental study on the aerodynamic performance degradation of a wind turbine blade model induced by ice accretion process, Renew. Energy 133 (2019) 663–675, https://doi.org/10.1016/j.renene.2018.10.032.
[4] D.L. Johnson, R.J. Erhardt, Projected impacts of climate change on wind energy density in the United States, Renew. Energy 85 (2016) 66–73, https://doi.org/10.1016/j.renene.2015.06.005.
[5] N. Dalili, A. Edrisy, R. Carriveau, A review of surface engineering issues critical to wind turbine performance, Renew. Sustain. Energy Rev. 13 (2009) 428–438, https://doi.org/10.1016/j.rser.2007.11.009.
[6] A. Zanon, M. De Gennaro, H. Kühnelt, Wind energy harnessing of the NREL 5 MW reference wind turbine in icing conditions under different operational strategies, Renew. Energy 115 (2018) 760–772, https://doi.org/10.1016/j.renene.2017.08.076.
[7] T. Wallenius, V. Lehtomäki, Overview of cold climate wind energy: challenges, solutions, and future needs, Wiley Interdiscip. Rev. Energy Environ. 5 (2016) 128–135, https://doi.org/10.1002/wene.170.
[8] W.J. Jasinski, S.C. Noe, M.S. Selig, M.B. Bragg, Wind turbine performance under icing conditions, J. Sol. Energy Eng. 120 (1998) 60, https://doi.org/10.1115/1.2888048.
[9] O. Parent, A. Ilinca, Anti-icing and de-icing techniques for wind turbines: critical review, Cold Reg. Sci. Technol. 65 (2011) 88–96, https://doi.org/10.1016/j.coldregions.2010.01.005.
[10] G. Fortin, J.-L. Laforte, A. Ilinca, Heat and mass transfer during ice accretion on aircraft wings with an improved roughness model, Int. J. Therm. Sci. 45 (2006) 595–606, https://doi.org/10.1016/j.ijthermalsci.2005.07.006.
[11] A.G. Kraj, E.L. Bibeau, Phases of icing on wind turbine blades characterized by ice accumulation, Renew. Energy 35 (2010) 966–972, https://doi.org/10.1016/j.renene.2009.09.013.

[12] M. Bragg, G. Gregorek, J. Lee, Airfoil aerodynamics in icing conditions, J. Aircraft 23 (1986) 76–81, https://doi.org/10.2514/3.45269 (accessed November 15, 2014).
[13] H. Habibi, L. Cheng, T. Zheng, V. Kappatos, C. Selcuk, T.-H. Gan, A dual de-icing system for wind turbine blades combining high-power ultrasonic guided waves and low-frequency forced vibrations, Renew. Energy 83 (2015) 859–870, https://doi.org/10.1016/J.RENENE.2015.05.025.
[14] J. Zeng, B. Song, Research on experiment and numerical simulation of ultrasonic de-icing for wind turbine blades, Renew. Energy 113 (2017) 706–712, https://doi.org/10.1016/j.renene.2017.06.045.
[15] S.K. Thomas, R.P. Cassoni, C.D. MacArthur, Aircraft anti-icing and de-icing techniques and modeling, J. Aircraft 33 (1996) 841–854, https://doi.org/10.2514/3.47027.
[16] L. Gao, Y. Liu, L. Ma, H. Hu, A hybrid strategy combining minimized leading-edge electric-heating and superhydro-/ice-phobic surface coating for wind turbine icing mitigation, Renew. Energy 140 (2019) 943–956, https://doi.org/10.1016/J.RENENE.2019.03.112.
[17] Y. Cheng, D. Rodak, C. Wong, C. Hayden, Effects of micro-and nano-structures on the self-cleaning behaviour of lotus leaves, Nanotechnology 17 (2006) 1359–1362. http://iopscience.iop.org/article/10.1088/0957-4484/17/5/032/meta (accessed February 14, 2016).
[18] Q. Liu, K.-T. Wu, M. Kobayashi, C.-K. Jen, N. Mrad, In-situ ice and structure thickness monitoring using integrated and flexible ultrasonic transducers, Smart Mater. Struct. 17 (2008) 45021–45023.
[19] L. Cao, A.K. Jones, V.K. Sikka, J. Wu, D. Gao, Anti-icing superhydrophobic coatings, Langmuir 25 (2009) 12444–12448, https://doi.org/10.1021/la902882b.
[20] L. Mishchenko, B. Hatton, V. Bahadur, Design of ice-free nanostructured surfaces based on repulsion of impacting water droplets, ACS Nano 4 (12) (2010) 7699–7707. http://pubs.acs.org/doi/abs/10.1021/nn102557p (accessed February 14, 2016.
[21] C. Antonini, F. Villa, M. Marengo, Oblique impacts of water drops onto hydrophobic and superhydrophobic surfaces: outcomes, timing, and rebound maps, Exp. Fluid 55 (2014) 1713, https://doi.org/10.1007/s00348-014-1713-9.
[22] A. Meuler, G. McKinley, R. Cohen, Exploiting topographical texture to impart icephobicity, ACS Nano 4 (2010) 7048–7052. http://pubs.acs.org/doi/abs/10.1021/nn103214q (accessed February 14, 2016).
[23] A. Cassie, S. Baxter, Wettability of porous surfaces, Trans. Faraday Soc. 40 (1944) 546–551. http://pubs.rsc.org/en/content/articlepdf/1944/tf/tf9444000546 (accessed February 14, 2016).
[24] R. Wenzel, Resistance of solid surface to wetting by water, Ind. Eng. Chem. (1936). http://pubs.acs.org/doi/pdf/10.1021/ie50320a024 (accessed September 11, 2017).
[25] M.A. Sarshar, C. Swarctz, S. Hunter, J. Simpson, C.-H. Choi, Effects of contact angle hysteresis on ice adhesion and growth on superhydrophobic surfaces under dynamic flow conditions, Colloid Polym. Sci. 291 (2013) 427–435, https://doi.org/10.1007/s00396-012-2753-4.
[26] J. Lv, Y. Song, L. Jiang, J. Wang, Bio-inspired strategies for anti-icing, ACS Nano (2014). http://pubs.acs.org/doi/abs/10.1021/nn406522n (accessed September 11, 2017).
[27] J. Soltis, J. Palacios, T. Eden, D. Wolfe, Ice adhesion mechanisms of erosion-resistant coatings, AIAA J. 53 (2015) 654–662, https://doi.org/10.2514/1.J053208.
[28] H. Baker, W.D. Bascom, C. Singleterry, The adhesion of ice to lubricated surfaces, J. Colloid Sci. 17 (1962) 477–491, https://doi.org/10.1016/0095-8522(62)90057-0.
[29] P. Kim, T.-S. Wong, J. Alvarenga, M.J. Kreder, W.E. Adorno-Martinez, J. Aizenberg, Liquid-infused nanostructured surfaces with extreme anti-ice and anti-frost performance, ACS Nano 6 (2012) 6569–6577, https://doi.org/10.1021/nn302310q.
[30] T.-S. Wong, S.H. Kang, S.K.Y. Tang, E.J. Smythe, B.D. Hatton, A. Grinthal, J. Aizenberg, Bioinspired self-repairing slippery surfaces with pressure-stable omniphobicity, Nature 477 (2011) 443–447, https://doi.org/10.1038/nature10447.
[31] H.F. Bohn, W. Federle, Insect aquaplaning: Nepenthes pitcher plants capture prey with the peristome, a fully wettable water-lubricated anisotropic surface, Proc. Natl. Acad. Sci. Unit. States Am. 101 (2004) 14138–14143, https://doi.org/10.1073/pnas.0405885101.
[32] T.-S. Wong, T. Sun, L. Feng, J. Aizenberg, Interfacial materials with special wettability, MRS Bull. 38 (2013) 366–371, https://doi.org/10.1557/mrs.2013.99.
[33] A.K. Epstein, T.-S. Wong, R.A. Belisle, E.M. Boggs, J. Aizenberg, Liquid-infused structured surfaces with exceptional anti-biofouling performance, Proc. Natl. Acad. Sci. Unit. States Am. 109 (2012) 13182–13187, https://doi.org/10.1073/pnas.1201973109.
[34] X. Dai, B.B. Stogin, S. Yang, T.-S. Wong, Slippery Wenzel state, ACS Nano 9 (2015) 9260–9267, https://doi.org/10.1021/acsnano.5b04151.
[35] P. Kim, T.-S. Wong, J. Alvarenga, M.J. Kreder, W.E. Adorno-Martinez, J. Aizenberg, Liquid-infused nanostructured surfaces with extreme anti-ice and anti-frost performance, ACS Nano 6 (2012) 6569–6577, https://doi.org/10.1021/nn302310q.
[36] J. Chen, R. Dou, D. Cui, Q. Zhang, Y. Zhang, F. Xu, X. Zhou, J. Wang, Y. Song, L. Jiang, Robust prototypical anti-icing coatings with a self-lubricating liquid water layer between ice and substrate, ACS Appl. Mater. Interfaces 5 (2013), https://doi.org/10.1021/am401004t, 130510105547001.
[37] J. Lv, Y. Song, L. Jiang, J. Wang, Bio-inspired strategies for anti-icing, ACS Nano 8 (2014) 3152–3169, https://doi.org/10.1021/nn406522n.
[38] P. Irajizad, M. Hasnain, N. Farokhnia, S.M. Sajadi, H. Ghasemi, Magnetic slippery extreme icephobic surfaces, Nat. Commun. 7 (2016) 13395, https://doi.org/10.1038/ncomms13395.
[39] K. Golovin, S.P.R. Kobaku, D.H. Lee, E.T. DiLoreto, J.M. Mabry, A. Tuteja, Designing durable icephobic surfaces, Sci. Adv. 2 (2016). http://advances.sciencemag.org/content/2/3/e1501496 (accessed September 9, 2017).
[40] D.L. Beemer, W. Wang, A.K. Kota, M. Doi, F. Brochard-Wyart, A. Tuteja, J. Aizenberg, J. Wang, Y. Song, L. Jiang, Durable gels with ultra-low adhesion to ice, J. Mater. Chem. A. 4 (2016) 18253–18258, https://doi.org/10.1039/C6TA07262C.
[41] X. Dai, N. Sun, S.O. Nielsen, B.B. Stogin, J. Wang, S. Yang, T.-S. Wong, Hydrophilic directional slippery rough surfaces for water harvesting, Sci. Adv. 4 (2018), eaaq0919, https://doi.org/10.1126/sciadv.aaq0919.
[42] G.K. Sirohia, X. Dai, Designing air-independent slippery rough surfaces for condensation, Int. J. Heat Mass Tran. 140 (2019) 777–785, https://doi.org/10.1016/j.ijheatmasstransfer.2019.06.035.
[43] Y. Liu, L. Ma, W. Wang, A.K. Kota, H. Hu, An experimental study on soft PDMS materials for aircraft icing mitigation, Appl. Surf. Sci. 447 (2018) 599–609, https://doi.org/10.1016/J.APSUSC.2018.04.032.
[44] L. Gao, R. Veerakumar, Y. Liu, H. Hu, Quantification of the 3D shapes of the ice structures accreted on a wind turbine airfoil model, J. Vis. 22 (2019) 661–667, https://doi.org/10.1007/s12650-019-00567-4.
[45] R.M. Waldman, H. Hu, High-speed imaging to quantify transient ice accretion process over an airfoil, J. Aircraft 53 (2015) 369–377, https://doi.org/10.2514/1.C033367.
[46] H. Sojoudi, M. Wang, N.D. Boscher, G.H. McKinley, K.K. Gleason, Z.Z. Yang, G.H. McKinley, K.K. Gleason, F. Liu, M.L. Hu, S.R. Hunter, J.A. Haynes, K.K. Gleason, Durable and scalable icephobic surfaces: similarities and distinctions from superhydrophobic surfaces, Soft Matter 12 (2016) 1938–1963, https://doi.org/10.1039/C5SM02295A.
[47] Q. Liu, Y. Yang, M. Huang, Y. Zhou, Y. Liu, X. Liang, Durability of a lubricant-infused Electrospray Silicon Rubber surface as an anti-icing coating, Appl. Surf. Sci. 346 (2015) 68–76, https://doi.org/10.1016/j.apsusc.2015.02.051.
[48] J.T. Korhonen, T. Huhtamäki, O. Ikkala, R.H.A. Ras, Reliable measurement of the receding contact angle, Langmuir 29 (2013) 3858–3863, https://doi.org/10.1021/la400009m.
[49] A.J. Meuler, J.D. Smith, K.K. Varanasi, J.M. Mabry, G.H. McKinley, R.E. Cohen, Relationships between water wettability and ice adhesion, ACS Appl. Mater. Interfaces 2 (2010) 3100–3110, https://doi.org/10.1021/am1006035.
[50] Z. Che, O.K. Matar, Impact of droplets on immiscible liquid films, Soft Matter 14 (2018) 1540–1551, https://doi.org/10.1039/c7sm02089a.
[51] L. Gordillo, T.-P. Sun, X. Cheng, Dynamics of drop impact on solid surfaces: evolution of impact force and self-similar spreading, J. Fluid Mech. 840 (2018) 190–214, https://doi.org/10.1017/jfm.2017.901.
[52] E. Ghabache, C. Josserand, T. Séon, Frozen impacted drop: from fragmentation to hierarchical crack patterns, Phys. Rev. Lett. 117 (2016), 074501, https://doi.org/10.1103/PhysRevLett.117.074501.
[53] Y. Liu, H. Hu, An experimental investigation on the unsteady heat transfer process over an ice accreting airfoil surface, Int. J. Heat Mass Tran. 122 (2018) 707–718, https://doi.org/10.1016/J.IJHEATMASSTRANSFER.2018.02.023.
[54] P. Zhang, F.Y. Lv, A review of the recent advances in superhydrophobic surfaces and the emerging energy-related applications, Energy 82 (2015) 1068–1087, https://doi.org/10.1016/j.energy.2015.01.061.